

~~GPU-HADVPPM4HIP V1.0: higher model accuracy on China's domestically GPU-like accelerator using heterogeneous compute interface for portability (HIP) technology to accelerate the piecewise parabolic method (PPM) in an air quality model (CAMx V6.10)~~

GPU-HADVPPM4HIP V1.0: using the heterogeneous interface for portability (HIP) to speed up the piecewise parabolic method in the CAMx (v6.10) air quality model on China's domestic GPU-like accelerator

Kai Cao¹, Qizhong Wu^{1,5}, Lingling Wang², Hengliang Guo³, Nan Wang², Huaqiong Cheng^{1,5},
Xiao Tang⁴, Dongxing Li^{1,5}, Lina Liu³, Dongqing Li¹, Hao Wu³, and Lanning Wang^{1,5}

¹College of Global Change and Earth System Science, Faculty of Geographical Science, Beijing Normal University, Beijing 100875, China

²Henan Ecological Environmental Monitoring Centre and Safety Center, Henan Key Laboratory of Environmental Monitoring Technology, Zhengzhou 450008, China

³National Supercomputing Center in Zhengzhou, Zhengzhou, 450001, China

⁴State Key Laboratory of Atmospheric Boundary Layer Physics and Atmospheric Chemistry, Institute of Atmospheric Physics, Chinese Academy of Science, Beijing 100029, China

⁵Joint Center for Earth System Modeling and High Performance Computing, Beijing Normal University, Beijing, 100875, China

Correspondence to: Qizhong Wu (wqizhong@bnu.edu.cn); Lingling Wang(928216422@qq.com);
Lanning Wang (wangln@bnu.edu.cn)

Abstract. The graphics processing units (GPUs) are becoming a compelling acceleration strategy for geoscience numerical model due to their powerful computing performance. In this study, AMD's heterogeneous compute interface for portability (HIP) was implemented to port the GPU

27 acceleration version of the Piecewise Parabolic Method (PPM) solver (GPU-HADVPPM) from
28 the NVIDIA GPUs to China's domestically GPU-like accelerators as GPU-HADVPPM4HIP, and
29 further introduced the multi-level hybrid parallelism scheme to improve the total computational
30 performance of the HIP version of CAMx (CAMx-HIP) model on the China's domestically
31 heterogeneous cluster. The experimental results show that the acceleration effect of GPU-
32 HADVPPM on the different GPU accelerator is more obvious when the computing scale is larger,
33 and the maximum speedup of GPU-HADVPPM on the domestic GPU-like accelerator is 28.9
34 times. The hybrid parallelism with a message passing interface (MPI) and HIP enables achieve up
35 to 17.2 times speedup when configure 32 CPU cores and GPU-like accelerators on the domestic
36 heterogeneous cluster. And the OpenMP technology is introduced to further reduce the
37 computation time of CAMx-HIP model by 1.9 times. More importantly, by comparing the
38 simulation results of GPU-HADVPPM on NVIDIA GPUs and domestic GPU-like accelerators, it
39 is found that the simulation results of GPU-HADVPPM on domestic GPU-like accelerators have
40 less difference than the NVIDIA GPUs, and the reason for this difference may be related to the
41 fact that the NVIDIA GPU loss part of the accuracy for improved computing performance. ~~All in
42 all, the domestic GPU-like accelerators are more accuracy for scientific computing in the field of
43 geoscience numerical models.~~ Furthermore, we also exhibit that the data transfer efficiency
44 between CPU and GPU has an important impact on heterogeneous computing, and point out that
45 optimizing the data transfer efficiency between CPU and GPU is one of the important directions to
46 improve the computing efficiency of geoscience numerical models in heterogeneous clusters in the
47 future.

48 1. Introduction

49 Over the recent years, GPUs have become an essential part of providing processing power for
50 high performance computing (HPC) application, and heterogeneous supercomputing based on
51 CPU processors and GPU accelerators has become the trend of global advanced supercomputing
52 development. ~~The 61st edition of the top 10 list, released in June 2023, reveals that 80% of
53 advanced supercomputers adopt the heterogeneous architectures
54 (<https://www.top500.org/lists/top500/2023/06/>, last access: 20 October 2023), and the Frontier~~

55 ~~system equipped with AMD Instinct MI250X GPU at the Oak Ridge National Laboratory remains~~
56 ~~the only true exascale machine with the High-Performance Linpack benchmark (HPL) score of~~
57 ~~1.194 Exaflop/s ([https://www.top500.org/news/frontier-remains-sole-exaflop-machine-and-](https://www.top500.org/news/frontier-remains-sole-exaflop-machine-and-keeps-top-spot-improving-upon-its-previous-hpl-score/)~~
58 ~~[retains top spot improving upon its previous hpl score/](https://www.top500.org/news/frontier-remains-sole-exaflop-machine-and-keeps-top-spot-improving-upon-its-previous-hpl-score/), last access: 20 October 2023).~~ It is worth
59 ~~noting that in addition to the second place Fugaku supercomputer using a general purpose CPU~~
60 ~~architecture, the third-ranked LUMI system also uses AMD Instinct MI250X GPUs as accelerators~~
61 ~~and its HPL score reaches 309.1 PFlop/s. The much watched AMD Instinct MI250X GPU~~
62 ~~achieves 95.7 TFlop/s for peak double precision matrix performance~~
63 ~~(<https://www.amd.com/en/products/server-accelerators/Instinct-mi250x>,~~ last access: 20 October
64 ~~2023), and its performance is 2.7 times that of EARTH SIMULATOR which is the top 1~~
65 ~~supercomputer in 2003. The 61st edition of the top 10 list, released in June 2023, reveals that 80%~~
66 ~~of advanced supercomputers adopt the heterogeneous architectures (Top500, 2023), and the~~
67 ~~Frontier system equipped with AMD Instinct MI250X GPU at the Oak Ridge National Laboratory~~
68 ~~remains the only true exascale machine with the High-Performance Linpack benchmark (HPL)~~
69 ~~score of 1.194 Exaflop/s (News, 2023). How to realize the large-scale parallel computing and~~
70 ~~improve the computational performance of geoscience numerical models on the GPU has become~~
71 ~~one of the significant directions for the future development of numerical models.~~

72 In terms of the heterogeneous porting for air quality model, most scholars select the chemical
73 module, one of the hotspots, to implement heterogeneous porting, and porting the computational
74 process originally on the CPU processes to the GPU accelerator, in order to improve the
75 computing efficiency.~~In terms of the heterogeneous porting for the atmospheric chemical models,~~
76 ~~many scholars have carried out research on chemical modules. For example, Sun et al. (2018) used~~
77 ~~CUDA technology to port the second-order Rosenbrock solver of chemistry module of CAM4-~~
78 ~~Chem to NVIDIA Tesla K20X GPU, and achieved up 11.7x speedup compared to the AMD~~
79 ~~Opteron™ 6274 (Interlagos) CPU (16 cores) using one CPU core.~~~~Sun et al. (2018) used CUDA~~
80 ~~technology to port the second-order Rosenbrock solver of chemistry module of CAM4-Chem to~~
81 ~~NVIDIA Tesla K20X GPU and achieved up 11.7x speedup for computation alone.~~ Alvanos and
82 Christoudias (2017) developed a software that automatically generates CUDA kernels to solve
83 chemical kinetics equation in the chemistry module for the global climate model ECHAM/MESSy

84 Atmospheric Chemistry (EMAC) and performance evaluation shows a 20.4x speedup for the
85 kernel execution. ~~Linford et al. (2011) presented the Kinesthetic PreProcessor: Accelerated (KPPA)~~
86 ~~to generate the chemical mechanism code in CUDA language which can be implemented on~~
87 ~~NVIDIA Tesla C1060 GPU. Linford et al. (2011) presented the Kinetic PreProcessor (KPP) to~~
88 ~~generate the chemical mechanism code in CUDA language which can be implemented on~~
89 ~~NVIDIA Tesla C1060 GPU. The KPP-generated SAPRC'99 mechanism from CMAQ model~~
90 ~~achieved a maximum speedup of 13.7x and KPP-generated RADM2 mechanism from WRF-chem~~
91 ~~model achieved an 8.5x speedup both compared to the Intel Quad-Core Xeon 5400 series~~
92 ~~CPU. The KPPA-generated SAPRC'99 mechanism from CMAQ model achieved a maximum~~
93 ~~speedup of 13.7x and KPPA-generated RADM2 mechanism from WRF-chem model achieved an~~
94 ~~8.5x speedup over the serial implementation. Similarly, the advection module is also one of the~~
95 ~~hotspot modules in the air quality model, Cao et al. (2023) adopted the Fortran-C-CUDA C~~
96 ~~scheme and implemented a series of optimizations, including reduction the CPU-GPU~~
97 ~~communication frequency, optimize the GPU memory access, and thread and block co-indexing,~~
98 ~~to increase the computational efficiency of the HADVPPM advection solver. It can achieve up to~~
99 ~~the 18.8x speedup on the NVIDIA Tesla V100 GPU compared to the Intel Xeon Platinum 8168~~
100 ~~CPU. Horizontal advection module for the atmospheric chemical models, Cao et al. (2023) used~~
101 ~~the Fortran-C-CUDA C scheme and implemented a series of optimizations, including reduce the~~
102 ~~CPU-GPU communication frequency, optimize the GPU memory access, and thread and block~~
103 ~~co-indexing, to increase the computational efficiency of the HADVPPM advection solver in the~~
104 ~~CAMx model by 18.8 times on the NVIDIA Tesla V100 GPU.~~

105 The CUDA technology was implemented to carry out heterogeneous porting for the
106 atmospheric chemical models from the CPU processors to different NVIDIA GPU
107 accelerators.~~The CUDA technology was implemented to carry out heterogeneous porting for the~~
108 ~~atmospheric chemical models from the CPU processors to different NIVIDA GPU accelerators. In~~
109 this study, the Heterogeneous-computing Interface for Portability (HIP) interface was introduced
110 to implement the porting of GPU-HADVPPM from the NVIDIA GPU to the China's domestically
111 GPU-like accelerators based on the research of Cao et al. (2023). The domestic GPU-like
112 accelerator plays the same role as the NVIDIA GPU, which is also used to accelerate the

113 ~~advection module in the CAMx model, so we refer to it as a GPU-like accelerator.~~In this study, the
114 ~~Heterogeneous computing Interface for Portability (HIP) interface was introduced to implement~~
115 ~~the porting of GPU-HADVPPM from the NVIDIA GPU to the China's domestically GPU-like~~
116 ~~accelerators based on the research of Cao et al. (2023).~~ First, we compared the simulation results
117 of the Fortran version CAMx model with the CAMx-CUDA and CAMx-HIP model which were
118 coupled with the CUDA and HIP versions of GPU-HADVPPM program, respectively.~~First, we~~
119 ~~compared the simulation result of the Fortran version CAMx model with the CUDA version of~~
120 ~~CAMx (CAMx-CUDA) and CAMx-HIP model which were coupled with the CUDA and HIP~~
121 ~~versions of GPU-HADVPPM program, respectively.~~First, we compared the simulation result of
122 Fortran version CAMx model with CUDA version of CAMx (CAMx-CUDA) and CAMx-HIP
123 model which were coupled with CUDA and HIP version of GPU-HADVPPM program,
124 respectively. ~~And then, the computing performance of GPU-HADVPPM programs on different~~
125 ~~GPUs were compared.~~And then, the computing performance of GPU-HADVPPM programs on
126 ~~different GPUs are compared.~~ Finally, we tested total coupling performance of CAMx-HIP model
127 with multi-level hybrid parallelization on the China's domestically heterogeneous cluster.

128 **2. Model and experimental platform**

129 **2.1. The CAMx model description and configuration**

130 ~~The Comprehensive Air Quality Model with Extensions version 6.10 (CAMx v6.10;~~
131 ~~ENVIRON, 2014) is a state-of-the-art air quality model which simulates the emission, dispersion,~~
132 ~~chemical reaction, and removal of the air pollutants on a system of nested three-dimensional grid~~
133 ~~boxes (<https://www.camx.com/>, last access: last access: 20 October 2023).~~The Comprehensive
134 Air Quality Model with Extensions version 6.10 (CAMx v6.10; ENVIRON, 2014) is a state-of-
135 the-art air quality model which simulates the emission, dispersion, chemical reaction, and removal
136 of the air pollutants on a system of nested three-dimensional grid boxes (CAMx, 2023). The
137 Eulerian continuity equation is expressed as shown Cao et al. (2023), the first term on the right-
138 hand side represents horizontal advection, the second term represents net resolved vertical
139 transport across an arbitrary space and time varying height grid, and the third term represents

140 turbulent diffusion on the sub-grid scale. Pollutant emission represents both point source
141 emissions and grided source emissions. Chemistry is treated by solving a set of reaction equations
142 defined by specific chemical mechanisms. Pollutant removal includes both dry deposition and wet
143 scavenging by precipitation.

144 In terms of the horizontal advection term on the right-hand side, this equation is solved using
145 either the Bott (1989) scheme or the Piecewise Parabolic Method (PPM) (Colella and Woodward,
146 1984; Odman and Ingram, 1996) scheme. The PPM horizontal advection scheme (HADVPPM)
147 was selected in this study because it provides higher accuracy with minimal numerical diffusion
148 (ENVIRON, 2014).~~The PPM horizontal advection scheme (HADVPPM) was selected in this~~
149 ~~study because it provides higher accuracy with minimal numerical diffusion.~~ The other numerical
150 schemes selected during the CAMx model testing are listed in Table S1.~~The other numerical~~
151 ~~scheme selected during the CAMx model running are listed in Table S1.~~ As described by Cao et al.
152 (2023), the -fp-model precise compile flag which can force the compiler to use the vectorization of
153 some computation under value safety is 41.4% faster than -mieee-fp compile flag which comes
154 from the Makefile of the official CAMx version with the absolute errors of the simulation results
155 are less than ± 0.05 ppbV. Therefore, the -fp-model precise compile flag was selected when
156 compiling the CAMx model in this research.

157 **2.2. CUDA and ROCm introduction**

158 Compute Unified Device Architecture (CUDA) (NVIDIA, 2020) is a parallel programming
159 paradigm which was released in 2007 by NVIDIA.~~CUDA is a proprietary application~~
160 ~~programming interface (API) and as such is only supported on NVIDIA's GPUs that are based on~~
161 ~~Tesla Architecture.~~ CUDA is a proprietary application programming interface (API) and as such is
162 only supported on NVIDIA's GPUs. For the CUDA programming, it uses a programming
163 language similar to standard C, which achieves efficient parallel computing of programs on
164 NVIDIA GPUs by adding some keywords. In the previous study, CUDA technology was
165 implemented to port the HADVPPM program from CPU to NVIDIA GPU (Cao et al., 2023).

166 Radeon Open Compute platform (ROCm) (AMD, 2023) is an open-source software platform
167 developed by AMD ~~in 2015~~ for HPC and hyperscale GPU computing. In general, ROCm for the

AMD GPU is equivalent to CUDA for NVIDIA GPU. On the ROCm software platform, it uses the AMD's HIP interface which is a C++ runtime API allowing developers to run programs on AMD GPUs. ~~On the ROCm software platform, it uses the AMD's HIP interface which is a C++ runtime API to allows developers to run programs on AMD GPUs.~~ Table 1 shows the difference between the CUDA programming and HIP programming on the NVIDIA GPU and AMD GPU. In general, they are very similar and their code can be converted directly by replacing the string "cuda" with "hip" in the most cases. ~~In general, it is very similar between the CUDA and HIP programming and their code can be converted directly by replacing the character "cuda" with "hip" in the most cases.~~ More information about HIP API can be available on <https://rocm.docs.amd.com/projects/HIP/en/latest/index.html> (last access: 20 October 2023). ~~More information about HIP API is available on the AMD ROCm website (ROCm, 2023).~~ Similar to AMD GPU, developers can also use ROCM-HIP programming interface to implement programs running on the China's domestically GPU-like accelerator. The CUDA code cannot run directly on domestic GPU-like accelerators, and it needs to be transcoded into HIP code. ~~Similar to AMD GPU, developers can also use ROCM-HIP programming interface to implement programs running on the China's domestically GPU-like accelerator.~~

Table 1. ~~The difference between the CUDA programming and HIP programming on the NVIDIA GPU and AMD GPU.~~

	CUDA programming	HIP programming
Header file	cuda_runtime.h	hip_runtime.h
Gets the number of compute capable GPUs.	cudaGetDeviceCount	hipGetDeviceCount
Set device to be used for GPU executions.	cudaSetDevice	hipSetDevice
Allocates memory on the GPU.	cudaMalloc	hipMalloc
Copies data between CPU and GPU.	cudaMemcpy	hipMemcpy
Kernel function	mykernel<<<>>>	hipLaunchKernelGGL(mykernel)
Frees memory on the GPU.	cudaFree	hipFree

2.3. Hardware components and software environment of the testing system

~~Table 2 listed four GPU clusters which are conducted the experiments, two NVIDIA heterogeneous clusters which have the same hardware configuration as Cao et al. (2023) and two~~

190 ~~China's domestically heterogeneous clusters newly used in this research. The NVIDIA K40m~~
191 ~~cluster is equipped with two 2.5 GHz 16 cores Intel Xeon E5-2682 v4 CPU and one NVIDIA~~
192 ~~Tesla K40m GPU. Each NVIDIA Tesla K40m GPU accelerator has 2880 CUDA cores with 12 GB~~
193 ~~of video memory. The NVIDIA V100 cluster contains two 2.7 GHz 24 cores Intel Xeon Platinum~~
194 ~~8168 processors and eight NVIDIA Tesla V100 GPU accelerators. Each NVIDIA Tesla V100 GPU~~
195 ~~accelerator is configured with 5120 CUDA cores and 16 GB video memory.~~

196 ~~For the China's domestically heterogeneous cluster A (domestic cluster A), each compute~~
197 ~~node contains a 2.0 GHz China's domestically CPU processor A of 32 cores (domestic CPU~~
198 ~~processor A) and four China's domestically GPU-like accelerator A (domestic GPU-like~~
199 ~~accelerator A). Each CPU processor A has 32 cores with 4 Non-Uniform Memory Access nodes,~~
200 ~~each NUMA node has 8 X86-based processors. The GPU-like accelerator A has 64 compute unit,~~
201 ~~for totaling 60 threads on each compute unit. The China's domestically heterogeneous cluster B~~
202 ~~(domestic cluster B) is the next generation of cluster A, and its CPU and GPU hardware have been~~
203 ~~upgraded, especially the data transfer bandwidth between CPU and GPU. The CPU and GPU~~
204 ~~configuration scheme on the cluster B is the same as the cluster B, with one 2.5 GHz China's~~
205 ~~domestically CPU processor B (domestic CPU processor B) on a single node equipped with four~~
206 ~~China's domestically GPU-like accelerator B (domestic GPU-like accelerator B). The domestic~~
207 ~~GPU-like accelerator B also contains 64 compute units with 128 threads each.~~

208 ~~In term of the software environment, the Intel Toolkit (including compiler and MPI library)~~
209 ~~version 2021.4.0, 2019.1.144, and 2021.3.0 are employed for compiling on Intel CPU and China's~~
210 ~~domestically series CPU, respectively. The drivers and libraries of NVIDIA Tesla K40m and V100~~
211 ~~GPU accelerator, domestic GPU-like accelerator A and B were CUDA version 10.2, CUDA~~
212 ~~version 10.0, ROCm version 4.0.1/ DTK toolkit version 23.04, and DTK toolkit version 23.04.~~
213 ~~DTK toolkit, like ROCm, supports developers to develop GPU-like applications using HIP~~
214 ~~programming interface in C++ language.~~

215 Table 1 lists four GPU clusters where we conducted the experiments, two NVIDIA
216 heterogeneous clusters which have the same hardware configuration as Cao et al. (2023) and two
217 China's domestically heterogeneous clusters newly used in this research, namely "Songshan"
218 supercomputer and "Taiyuan" computing platform. Two NVIDIA heterogeneous clusters are

219 equipped with NVIDIA Tesla K40m and V100 GPU accelerators, respectively. Both two domestic
 220 clusters include thousands of computing nodes and each containing one China’ s domestically
 221 CPU processor, four China’ s domestically GPU-like accelerators, and 128 GB of DDR4 2666
 222 memory. The domestic CPU has four NUMA nodes, each NUMA node has eight X86 based
 223 processors. The accelerator adopts a GPU-like architecture consisting of a 16 GB HBM2 device
 224 memory and many compute units. The GPU-like accelerators connected to CPU with PCI-E, the
 225 peak bandwidth of the data transfer between main memory and device memory is 16 GB/s.

226 It is worth noting that the “Taiyuan” computing platform, which has been updated in three
 227 main aspects compared to the “Songshan” supercomputer. The CPU clock speed has been
 228 increased from 2.0 GHz to 2.5 GHz, the number of GPU-like computing units has been increased
 229 from 3,840 to 8,192, and the peak bandwidth between main memory and video memory has been
 230 increased from 16 GB/s to 32 GB/s. In terms of the software environment, in addition, the NVIDA
 231 GPU is programmed using the CUDA toolkit, and the domestic GPU-like is programmed using
 232 the ROCm-HIP toolkit developed by AMD in 2015 for HPC and hyper-scale GPU computing
 233 (ROCm, 2023). On the ROCm software platform, it uses the AMD’s HIP interface to allow
 234 developers to run programs on Chinese GPU-like accelerators. More details about the hardware
 235 composition and software environment of the four heterogeneous clusters are presented in Table 1.

236 **Table 1.** Configurations of the NVIDIA K40m cluster, NVIDIA V100 cluster, “Songshan” supercomputer, and
 237 “Taiyuan” computing platform.

	Hardware components	
	CPU	GPU
<u>NVIDIA K40m cluster</u>	<u>Intel Xeon E5-2682 v4 CPU @2.5 GHz, 16 cores</u>	<u>NVIDIA Tesla K40m GPU, 2880 CUDA cores, 12 GB video memory</u>
<u>NVIDIA V100 cluster</u>	<u>Intel Xeon Platinum 8168 CPU @2.7 GHz, 24 cores</u>	<u>NVIDIA Tesla V100 GPU, 5120 CUDA cores, 16 GB video memory</u>
<u>Songshan supercomputer</u>	<u>China’ s domestically CPU processor A, 2.0GHz, 32 cores</u>	<u>China’ s domestically GPU-like accelerator A, 3840 computing units, 16 GB memory</u>
<u>Taiyuan computing platform</u>	<u>China’ s domestically CPU processor B, 2.5GHz, 32 cores</u>	<u>China’ s domestically GPU-like accelerator B, 8192 computing units, 16 GB memory</u>
	Software environment	
	Compiler and MPI	Programming model
<u>NVIDIA K40m cluster</u>	<u>Intel Toolkit 2021.4.0</u>	<u>CUDA-10.2</u>
<u>NVIDIA V100 cluster</u>	<u>Intel Toolkit 2019.1.144</u>	<u>CUDA-10.0</u>
<u>Songshan supercomputer</u>	<u>Intel Toolkit 2021.3.0</u>	<u>ROCm-4.0.1/DTK-23.04</u>

238 **Table 2.** Configurations of NVIDIA K40m cluster, NVIDIA V100 cluster, China’s domestically cluster A, and
 239 China’s domestically cluster B.

	Hardware components	
	CPU	GPU
NVIDIA K40m cluster	Intel Xeon E5-2682 v4 CPU @2.5 GHz, 16 cores	NVIDIA Tesla K40m GPU, 2880 CUDA cores, 12 GB video memory
NVIDIA V100 cluster	Intel Xeon Platinum 8168 CPU @2.7 GHz, 24 cores	NVIDIA Tesla V100 GPU, 5120 CUDA cores, 16 GB video memory
China’s domestically cluster A	China’s domestically CPU processor A, 2.0GHz, 32 cores	China’s domestically GPU-like accelerator A, 3840 computing units, 16 GB memory
China’s domestically cluster B	China’s domestically CPU processor B, 2.5GHz, 32 cores	China’s domestically GPU-like accelerator B, 8192 computing units, 16 GB memory
	Software environment	
	Compiler and MPI	Programming model
NVIDIA K40m cluster	Intel Toolkit 2021.4.0	CUDA 10.2
NVIDIA V100 cluster	Intel Toolkit 2019.1.144	CUDA 10.0
China’s domestically cluster A	Intel Toolkit 2021.3.0	ROCm 4.0.1/DTK 23.04
China’s domestically cluster B	Intel Toolkit 2021.3.0	DTK 23.04

240

241 **3. Implementation details**

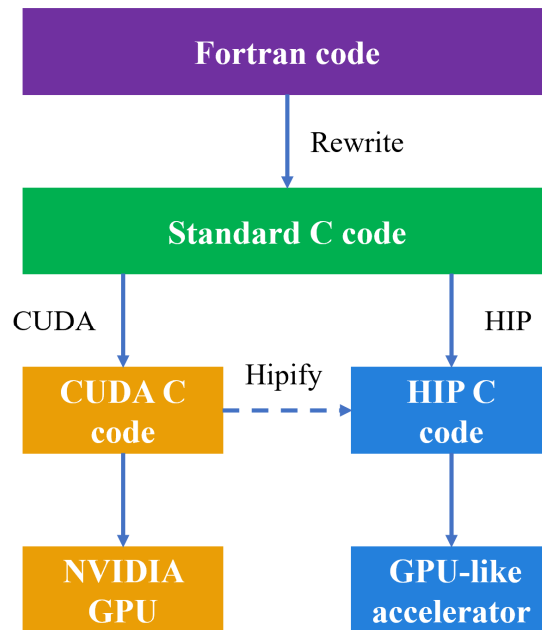
242 This section mainly introduced the strategy of porting HADVPPM program from CPU to
 243 NVIDIA GPU and domestic GPU-like accelerator, as well as the proposed multi-level hybrid
 244 parallelism technology to make full use of computing resources.

245 **3.1. Porting the HADVPPM program from CPU to NVIDIA GPU and domestic**
 246 **GPU-like accelerator**

247 Fig. 1 shows the heterogeneous porting process of HADVPPM from CPU to NVIDIA GPU
 248 and domestic GPU-like accelerator. First, the original Fortran code was refactored using standard
 249 C language. And then the CUDA and HIP technology were used to convert the standard C code
 250 into CUDA C and HIP C code to make it computable on the NVIDIA GPU and domestic GPU-
 251 like accelerator. To facilitate the portability of applications across different GPU platforms, ROCm
 252 provides hipify toolkits to help transcode. In this studying, the ROCm HIP technology was used to

253 ~~implement the operation of GPU-HADVPPM on domestic GPU-like accelerator based on the~~
254 ~~CUDA version of GPU-HADVPPM which was developed by Cao et al. (2023). During the~~
255 ~~compiling, the HIP code was compiled using the “hipcc” compiler driver with the library flag “-~~
256 ~~lamdhip64”.~~

257 Fig. 1 shows the heterogeneous porting process of HADVPPM from CPU to NVIDIA GPU
258 and domestic GPU-like accelerator. First, the original Fortran code was refactored using standard
259 C language. Then the CUDA and ROCm-HIP technology were used to convert the standard C
260 code into CUDA C and HIP C code to make it computable on the NVIDIA GPU and domestic
261 GPU-like accelerator. Similar to CUDA technology, the HIP technology is implemented to convert
262 the standard C code to HIP C code by adding related built-in functions (such as hipMalloc,
263 hipMemcpy, hipFree, etc.). To facilitate the portability of applications across different GPU
264 platforms, ROCm provides hipify toolkits to help transcode. The hipify toolkit is essentially a
265 simple script written in the Perl language, and its function is text replacement, which replaces the
266 function name in CUDA C code with the corresponding name in HIP C code according to certain
267 rules. For example, for the memory allocation function cudaMalloc in CUDA, the hipify toolkit
268 can automatically recognize and replace it with hipMalloc. Therefore, the thread and block
269 configuration of GPU remain unchanged due to the simple text substitution during the transcoding.
270 In this study, the ROCm HIP technology was used to implement the operation of GPU-
271 HADVPPM on domestic GPU-like accelerator based on the CUDA version of GPU-HADVPPM
272 which was developed by Cao et al. (2023). The HIP code was compiled using the “hipcc”
273 compiler driver with the library flag “-lamdhip64”.



274

275 **Figure 1.** The heterogeneous porting process of HADVPPM Fortran code from CPU to NVIDIA GPU and
 276 domestic GPU-like accelerator.

277

278 **3.2. Multi-level hybrid parallelization of CAMx model on heterogeneous**
 279 **platform**

280 The original CAMx model running on the CPUs supports two types of parallelization
 281 (ENVIRON, 2014): (1) OpenMP (OMP), which supports multi-platform (e.g., multi-core) shared-
 282 memory programming in C/C++ and Fortran; (2) Message Passing Interface (MPI), which is a
 283 message passing interface standard for developing and running parallel applications on the
 284 distributed-memory computer cluster. During the process of CAMx model simulation, MPI and
 285 OMP hybrid parallelism can be used, several CPU processes can be launched, and each process
 286 can spawn several threads. This hybrid parallelism can significantly improve the computational
 287 efficiency of CAMx model.~~In the process of CAMx simulation, using MPI and OMP hybrid~~
 288 ~~parallelism, several CPU processes can be launched, and each process can spawn several threads.~~
 289 This hybrid parallelism can significantly improve the computational efficiency of CAMx model.~~In~~

290 ~~the original CAMx model, MPI+OMP hybrid parallel can be used to maximize computational~~
291 ~~efficiency.~~

292 ~~As mentioned above, the original CAMx model supports message passing interface (MPI)~~
293 ~~parallel technology running on the general-purpose CPU. The simulation domain is divided into~~
294 ~~several sub-regions by MPI, and each CPU process is responsible for computation of its sub-~~
295 ~~region, which includes the computation tasks of advection module and other modules such as~~
296 ~~photolysis module, deposition module, chemical module, etc. The simulation domain is divided~~
297 ~~into several sub-regions by MPI, and each CPU process is responsible for simulation of its sub-~~
298 ~~region, which includes advection module and other modules such as photolysis module, deposition~~
299 ~~module, chemical module, etc. In the previous studying, Cao et al. (2023) adopt a parallel~~
300 ~~architecture with an MPI and CUDA (MPI+CUDA) hybrid paradigm to configure one GPU~~
301 ~~accelerator for each CPU process. For the advection module, the simulation originally~~
302 ~~implemented by the CPU is handed over to the GPU. Other module computing tasks continue to~~
303 ~~be completed on the CPU.~~

304 ~~In this study, when the CUDA C code of GPU-HADVPPM is converted to HIP C code, GPU-~~
305 ~~HADVPPM with an MPI and HIP (MPI+HIP) heterogeneous hybrid programming technology can~~
306 ~~also run on multiple domestic GPU-like accelerators. The MPI and HIP hybrid parallel scheme~~
307 ~~can also configure one GPU-like accelerator for each CPU process. However, the number of GPU-~~
308 ~~like accelerators in a single compute node is usually much smaller than the number of CPU cores~~
309 ~~in the heterogeneous HPC systems. Therefore, in order to make full use of the remaining CPU~~
310 ~~computing resources, the OMP API of CAMx model is further introduced to realize the~~
311 ~~MPI+OMP hybrid parallelism of other modules on CPU. Therefore, in order to make full use of the~~
312 ~~remaining CPU computing resources, the OpenMP (OMP) hybrid parallel framework of CAMx~~
313 ~~model is further introduced to realize the MPI+OMP hybrid parallelism of other modules on CPU.~~
314 ~~A schematic of the multi-level hybrid parallel framework is shown in Figure 2. For example, in a~~
315 ~~computing node, four CPU processes and four GPU-like accelerators are launched, and each CPU~~
316 ~~process spawns four threads. Then the advection module is simulated by 4 GPU-like accelerators,~~
317 ~~and the other modules are done by 4*4 threads spawned by CPU processes.~~

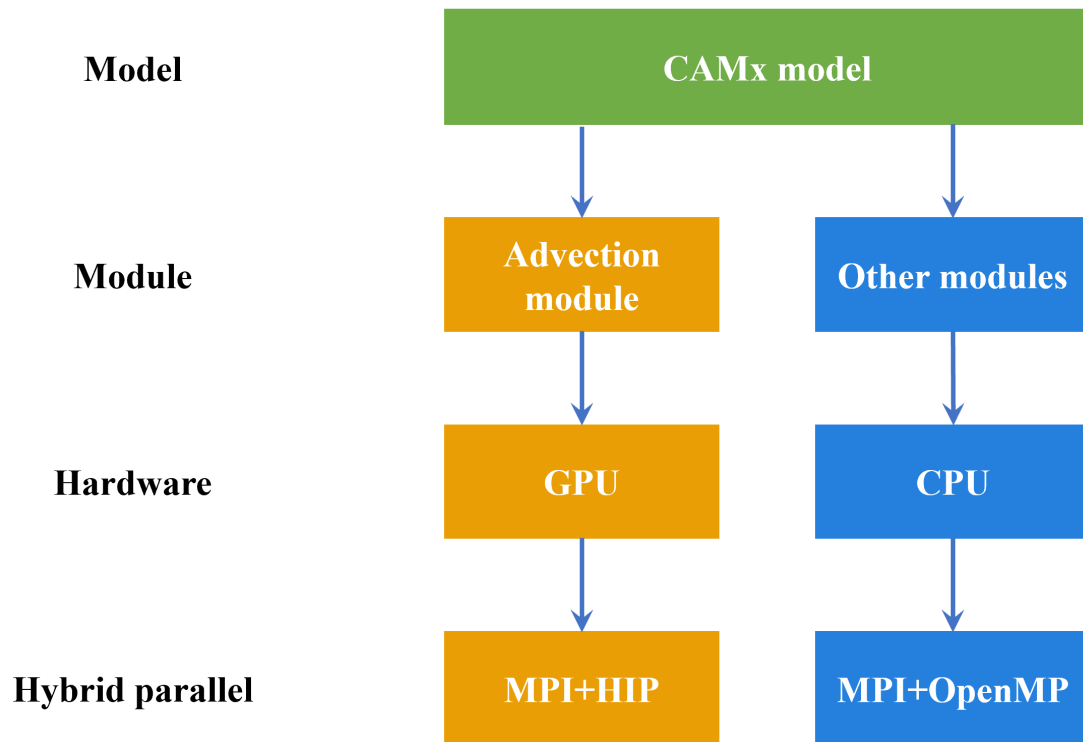


Figure 2. A schematic of the multi-level hybrid parallel framework.

In the previous studying, Cao et al. (2023) adopt a parallel architecture with an MPI and CUDA (MPI+CUDA) hybrid paradigm to expand the parallel scale of CAMx-CUDA model in NVIDIA heterogeneous cluster. Adopting this strategy, GPU-HADVPPM can run on multiple NVIDIA-GPUs. When the CUDA-C code of GPU-HADVPPM is converted to HIP-C code, GPU-HADVPPM with an MPI and HIP (MPI+HIP) heterogeneous hybrid programming technology can also run on multiple domestic GPU-like accelerators. The MPI and HIP hybrid parallel scheme can configure one GPU-like accelerator for each CPU process participating in the computation. However, the number of GPU-like accelerators in a single compute node is usually much smaller than the number of CPU cores in the super-large heterogeneous cluster. Therefore, in order to make full use of the remaining CPU computing resources, OMP technology is further introduced into the CAMx-HIP model which was coupled the HIP version of GPU-HADVPPM. In the framework of the multi-level hybrid parallelism, the horizontal advection module is accelerated by MPI and HIP technology, and the other modules are accelerated by MPI and OMP.

333 4. Results and evaluation

334 ~~The computational coupling performance experiments of CUDA and HIP version GPU-~~
335 ~~HADVPPM are reported in this section. The coupling performance experiments of CUDA and HIP~~
336 ~~version GPU-HADVPPM were conducted in this section. First, we compared the simulation result~~
337 ~~of the Fortran version CAMx model with CAMx-CUDA and CAMx-HIP model which were~~
338 ~~coupled with CUDA and HIP version of GPU-HADVPPM program, respectively. First, we~~
339 ~~compared the simulation result of Fortran version CAMx model with CAMx-CUDA and CAMx-~~
340 ~~HIP model which were coupled with CUDA and HIP version of GPU HADVPPM program,~~
341 ~~respectively.~~ Then, the computational computing performance of GPU-HADVPPM programs on
342 the NVIDIA GPU and domestic GPU-like accelerator are compared. Finally, we tested total
343 coupling performance of CAMx-HIP model with multi-level hybrid parallelization on the the
344 "Songshan" supercomputer domestic cluster A. For ease of description, the CAMx versions of the
345 HADVPPM program written in Fortran, CUDA C and HIP C code are named Fortran, CUDA and
346 HIP, respectively.

347 4.1. Experimental setup

348 ~~There are three test cases were used to evaluate the coupling performance of CUDA and HIP~~
349 ~~version GPU-HADVPPM. The experimental setup for the three test cases is shown in Table 2. In~~
350 ~~the previous study of Cao et al. (2023), we only used BJ case to carry out the performance tests.~~
351 ~~HN case and ZY case are the newly constructed test cases in this study. The Beijing case (BJ)~~
352 ~~covers Beijing, Tianjin, and part of the Hebei Province with 145×157 grid boxes, and simulation~~
353 ~~of BJ case starts on 1 November, 2020. The Henan case (HN) mainly covers the Henan Province~~
354 ~~with 209×209 grid boxes. The starting date of simulation in HN case is 1 October, 2022. The~~
355 ~~Zhongyuan case (ZY) has the widest coverage of the three cases, with Henan Province as the~~
356 ~~center, covering the Beijing-Tianjin-Hebei region, Shanxi Province, Shaanxi Province, Hubei~~
357 ~~Province, Anhui Province, Jiangsu Province, and Shandong Province, with 531×513 grid boxes.~~
358 ~~ZY case started simulation on 4 January, 2023. There are three test cases were used to evaluate the~~
359 ~~coupling performance of CUDA and HIP version GPU-HADVPPM. The experimental setup for~~
360 ~~the three test cases is shown in Table 3. The Beijing case (BJ) covers Beijing, Tianjin, and part of~~

361 ~~the Hebei Province with 145 × 157 grid boxes, and simulation of BJ case starts on 1 November,~~
362 ~~2020. The Henan case (HN) mainly covers the Henan Province with 209 × 209 grid boxes. The~~
363 ~~starting date of simulation in HN case is 1 October, 2022. The Zhongyuan case (ZY) has the~~
364 ~~widest coverage of the three cases, with Henan Province as the center, covering the Beijing-~~
365 ~~Tianjin-Hebei region, Shanxi Province, Shaanxi Province, Hubei Province, Anhui Province,~~
366 ~~Jiangsu Province, and Shandong Province, with 531 × 513 grid boxes. ZY case started simulation~~
367 ~~on 4 January, 2023.~~ All of the three performance test cases are 3km horizontal resolution, 48 hours
368 of simulation, and 14 vertical model layers. The number of three-dimensional grid boxes in BJ,
369 HN, and ZY cases are totally 318,710, 611,534 and 3,813,642, respectively. The meteorological
370 fields inputting the different versions of the CAMx model in the three cases were provided by the
371 Weather Research and Forecasting Model (WRF). In terms of emission inventories, the emission
372 for BJ case is consistent with the Cao et al. (2023), HN case uses the Multi-resolution Emission
373 Inventory for China (MEIC) and ZY case uses the emission constructed by Sparse Matrix
374 Operator Kernel Emission (SMOKE) model in this study.

375 **Table 23.** The experimental setup for the BJ, HN, and ZY case.

	BJ	HN	ZY
Start date	November 1, 2020	October 1, 2022	1 January, 2023
Horizontal resolution	3km	3km	3km
Grid boxes	145 × 157 × 14	209 × 209 × 14	531 × 513 × 14
Meteorological fields	WRF	WRF	WRF
Emission	Cao et al. (2023)	MEIC	SMOKE

376

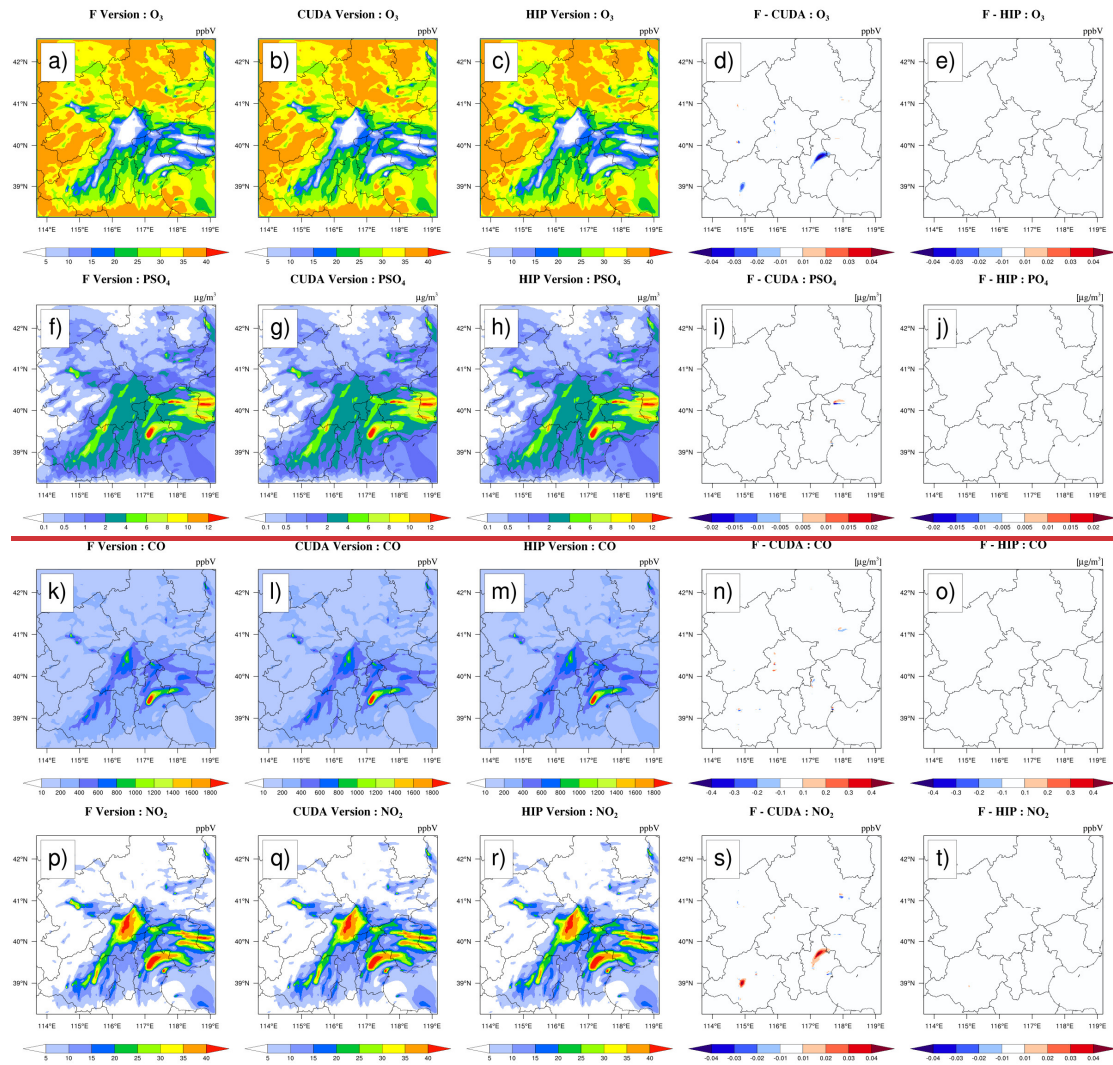
377 4.2. Error analysis

378 The hourly concentrations of four major species, i.e. O₃, PSO₄, CO, and NO₂, outputted by
379 the Fortran, CUDA, and HIP versions of CAMx for the BJ case are compared to verify the results
380 correctness before testing the computational performance.~~The hourly concentrations of four major~~
381 ~~species, i.e. O₃, PSO₄, CO, and NO₂, outputted by Fortran, CUDA, and HIP version of CAMx for~~
382 ~~the BJ case are compared to verify the results reasonableness before testing the computation~~
383 ~~performance. Fig. 32 shows the four major species simulation results of the three CAMx version,~~
384 including Fortran version on the Intel E5-2682 v4 CPU, CUDA version on the NVIDIA K40m

385 cluster and HIP version on the “Songshan” supercomputer, after 48 hours integration, as well as
386 the absolute errors (AEs) of their concentrations. Fig. 2 present the four major species simulation
387 results of three CAMx version, including Fortran version on the Intel E5-2682 v4 CPU, CUDA
388 version on the NVIDIA K40m cluster and HIP version on the domestic cluster A, after 48 hours
389 integration, as well as the absolute errors (AEs) of their concentrations. As described by Cao et al.
390 (2023)As mentioned above, the parallel design of the CAMx model adopts the primary/secondary
391 mode, and P0 process is responsible for inputting and outputting the data and calling the
392 MPI_Barrier function to synchronize the process, and the other processes are responsible for
393 simulation. When comparing the simulation results, we only launched 2 CPU processes on the
394 CPU platform, and launched 2 CPU processes and configure 2 GPU accelerators on the NVIDIA
395 K40m cluster and “Songshan” supercomputer, respectively.

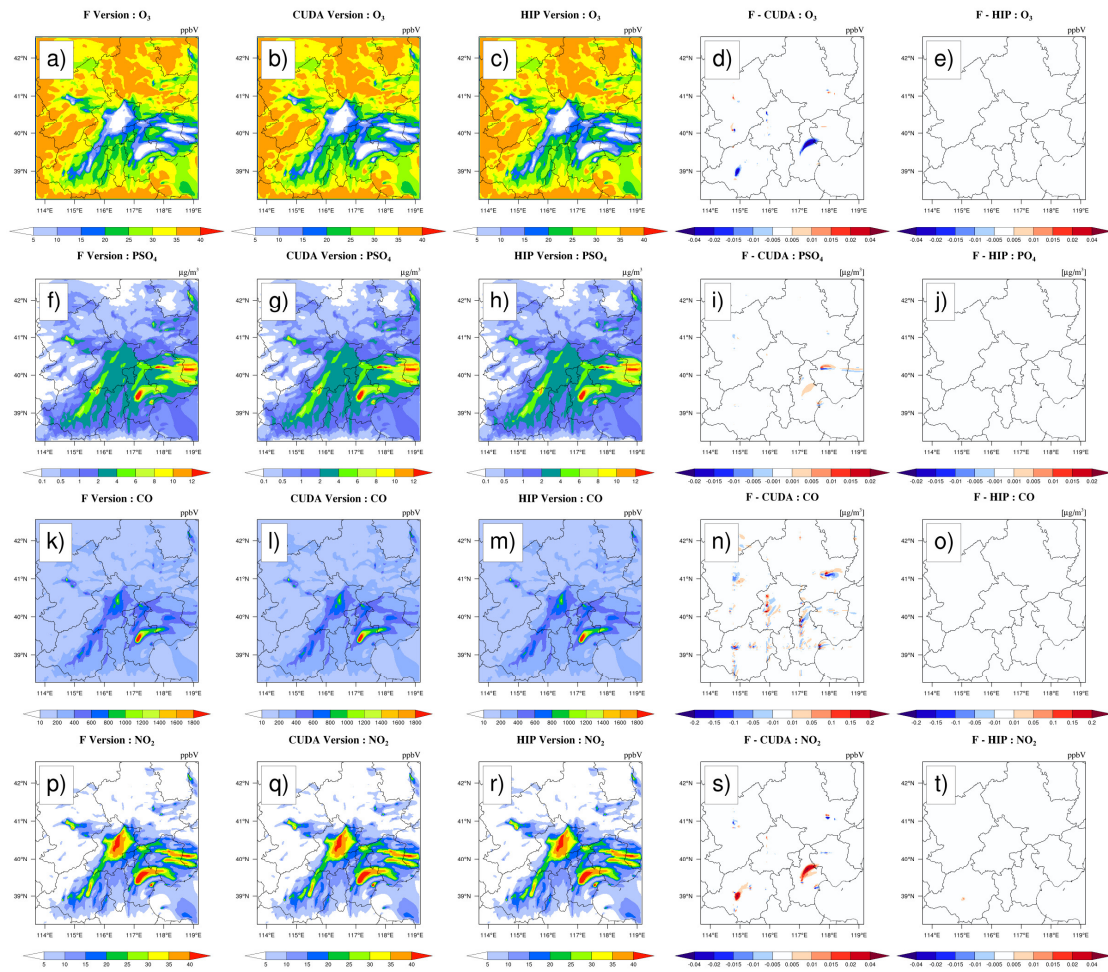
396 The species’ spatial pattern of three CAMx versions on different platform are visually very
397 consistent, and the AEs between the HIP and Fortran version is much smaller than the CUDA and
398 Fortran version. For example, the AEs between the CUDA and Fortran version for O₃, PSO₄, and
399 NO₂ are in the range of ± 0.04 ppbV, $\pm 0.02 \mu\text{g} \cdot \text{m}^{-3}$, and ± 0.04 ppbV. And the AEs between the
400 HIP and Fortran version for above the three species are fall into the range of ± 0.01 ppbV, ± 0.005
401 $\mu\text{g} \cdot \text{m}^{-3}$, and ± 0.01 ppbV. For CO, AEs is relatively large due to its high background
402 concentration. However, the AEs between the HIP and Fortran versions is also less than that
403 between the CUDA and Fortran versions where were in the range of ± 0.4 ppbV and ± 0.1 ppbV,
404 respectively.

405 Considering the situation of AEs accumulate and grow, Figure 43 highlights the time series of
406 AEs between Fortran and CUDA versions and between Fortran and HIP versions after grid
407 averaging. As is shown in Fig. 43, the AEs of O₃, PSO₄, CO, and NO₂ between the Fortran version
408 and the CUDA version are -0.0002 to 0.0001 ppbV, -0.00003 to 0.00001 $\mu\text{g} \cdot \text{m}^{-3}$, -0.0004 to
409 0.0004 ppbV, and -0.0002 to 0.0002 ppbV, respectively, and fluctuate. Although the AEs of the
410 above four species between the Fortran and the HIP version also fluctuates, the fluctuation range
411 is much smaller than that of the CUDA version. Importantly, the AEs between Fortran and CUDA
412 versions and between Fortran and HIP versions both do not accumulate and grow over prolonged
413 simulation periods.



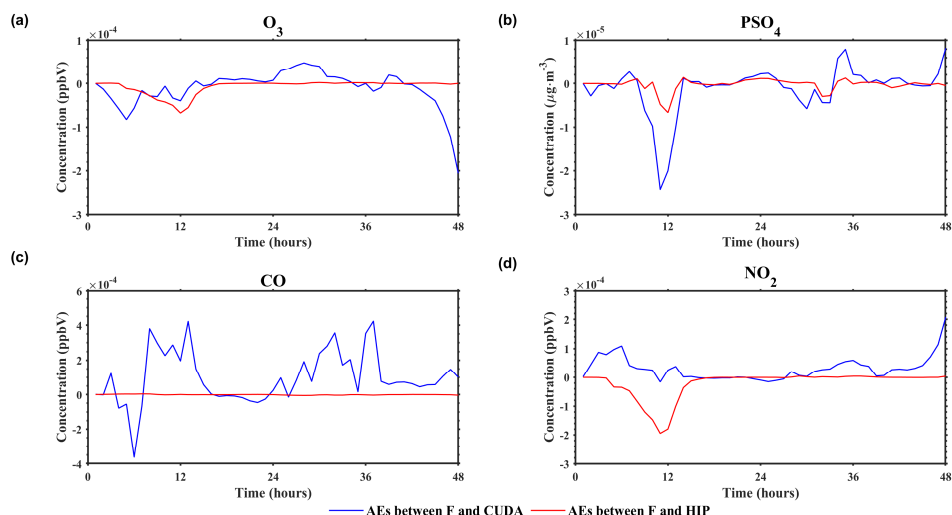
414

415



416

417 **Figure 32.** O₃, PSO₄, CO, and NO₂ concentrations outputted by the CAMx Fortran version on the Intel E5-2682 v4
 418 CPU, CUDA version on the NVIDIA K40m cluster and HIP version on the "Songshan" supercomputer
 419 domestic cluster A under the BJ case. Panels (a), (f), (k), and (p) are from the Fortran version of simulation results
 420 for four species. Panels (b), (g), (l), and (q) are from the CUDA version of simulation results for four species.
 421 Panels (c), (h), (m), and (r) are from the HIP version of simulation results for four species. Panels (d), (i), (n), and
 422 (s) are the AEs between the Fortran and CUDA versions. Panels (e), (j), (o), and (t) are the AEs between the
 423 Fortran and HIP versions.

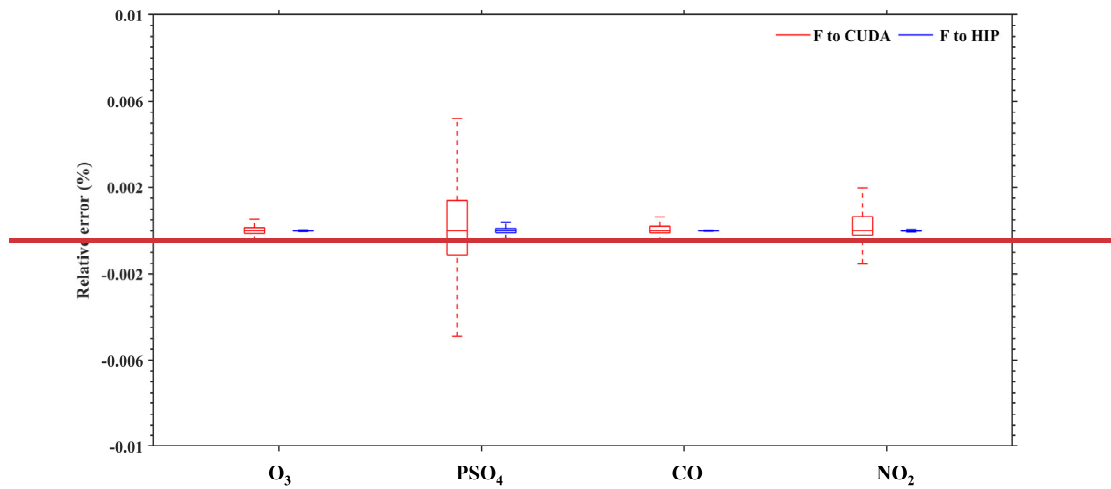


424

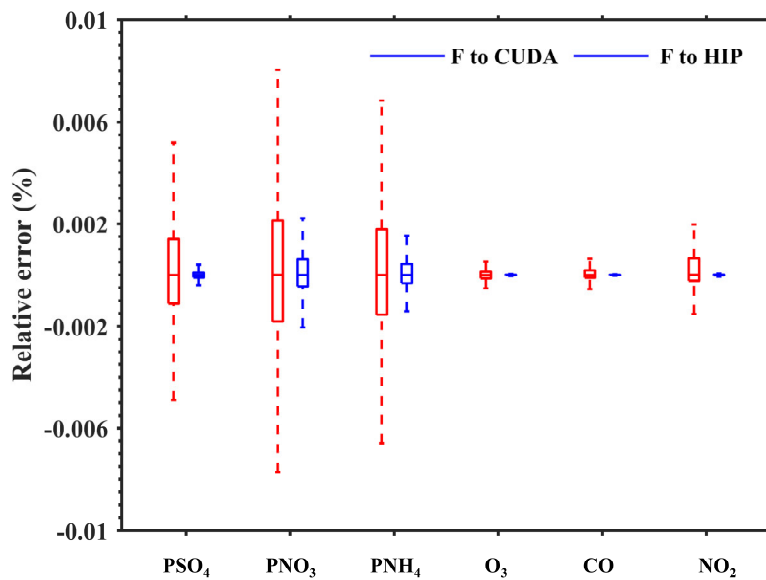
425 **Figure 43.** The time series of AEs between Fortran and CUDA versions (solid blue line) and between Fortran and
 426 HIP versions (solid red line) after grid averaging. Panel (a)–(d) represent the AEs of O_3 , PSO_4 , CO , and NO_2 ,
 427 respectively.

428 **Fig. 53** presents the boxplot of the relative errors (REs) in all grid boxes for the PSO_4 , PNO_3 ,
 429 PNH_4 , O_3 , CO , and NO_2 during the 48 hours simulation under the BJ case. Statistically, the REs
 430 between the CUDA version on the NVIDIA K40m cluster and Fortran version on the Intel E5-
 431 2682 v4 CPU for the above six species are in the range of $\pm 0.006\%$, $\pm 0.01\%$, $\pm 0.008\%$,
 432 $\pm 0.002\%$, $\pm 0.002\%$, and $\pm 0.002\%$. In terms of REs between the HIP version on the “Songshan”
 433 supercomputer and Fortran version on the Intel E5-2682 v4 CPU, the values are much smaller
 434 than REs between CUDA and Fortran versions which are fall into the range of $\pm 0.0005\%$,
 435 $\pm 0.004\%$, $\pm 0.004\%$, $\pm 0.00006\%$, $\pm 0.00004\%$, and $\pm 0.00008\%$, respectively. In the air quality
 436 model, the secondary particulate matter, such as PNH_4 , PNO_3 , and PSO_4 , have a common
 437 characteristic: their initial concentration is very low and they are mainly generated through
 438 complex chemical reactions. Therefore, when calculating the relative error on different hardware
 439 platforms, because the value in the denominator is very small, it is very sensitive to a small
 440 difference in the numerator, resulting in a large relative error. But from the absolute error in Fig.34,
 441 the absolute error of PSO_4 on different hardware platforms is smaller than that of other species.
 442 For gaseous pollutants such as CO , O_3 , and NO_2 , the initial concentration is large due to emission,
 443 and the denominator value is large when calculating the relative error, which is insensitive to small
 444 differences in the numerator. Fig. 3 presents the boxplot of the relative errors (REs) in all grid
 445 boxes for the O_3 , PSO_4 , CO , and NO_2 during the 48 hours simulation under the BJ case.

446 ~~Statistically, the REs between the CUDA version on the NVIDIA K40m cluster and Fortran~~
 447 ~~version on the Intel E5-2682 v4 CPU for the above four species are in the range of $\pm 0.002\%$,~~
 448 ~~$\pm 0.006\%$, $\pm 0.002\%$, and $\pm 0.002\%$. In terms of REs between the HIP version on the domestic~~
 449 ~~cluster A and Fortran version on the Intel E5-2682 v4 CPU, the values are much smaller than REs~~
 450 ~~between CUDA and Fortran versions which are fall into the range of $\pm 0.00006\%$, $\pm 0.0005\%$,~~
 451 ~~$\pm 0.00004\%$, and $\pm 0.00008\%$, respectively.~~



452



453

454 **Figure 5.43**—The distribution of REs in all grid boxes for the PSO₄, PNO₃, PNH₄, O₃, CO, and NO₂ under the BJ
 455 case. The red boxplot represents the REs between the CUDA version on the NVIDIA K40m cluster and Fortran

456 [version on the Intel E5-2682 v4 CPU, and blue boxplot represents the REs between the HIP version on the](#)
457 ["Songshan" supercomputer and Fortran version on the Intel E5-2682 v4 CPU.](#)

458 ~~The distribution of REs in all grid boxes for the O₃, PSO₄, CO, and NO₂ under the BJ case. The red boxplot~~
459 ~~represents the REs between the CUDA version on the NVIDIA K40m cluster and Fortran version on the Intel E5-~~
460 ~~2682 v4 CPU, and blue boxplot represents the REs between the domestic cluster A and Fortran version on the Intel~~
461 ~~E5-2682 v4 CPU.~~

462 Wang et al. (2021) verified the applicability of the numerical model in scientific research by
463 computing the ratio of root mean square error (RMSE) between two different model versions to
464 system spatial variation (standard deviation, std). If the ratio is smaller, it is indicated that the
465 difference in the simulation results of the model on the GPU is minimal compared with the spatial
466 variation of the system, that is to say, the simulation results of the model on the GPU are accepted
467 for scientific research. Here, we ~~calculate~~[compute](#) the standard deviation of O₃, PSO₄, CO and
468 NO₂ on the Intel Xeon E5-2682 v4 CPU, and their ~~root mean square error (RMSE)~~ between the
469 NVIDIA V100 cluster, NVIDIA K40m cluster and ~~"Songshan" supercomputer~~[domestic cluster A](#)
470 and the Intel Xeon E5-2682 v4 CPU, which are presented in Table [34](#). The std for the above four
471 species on the Intel Xeon E5-2682 v4 CPU are 9.6 ppbV, $1.7 \mu\text{g} \cdot \text{m}^{-3}$, 141.9 ppbV, and 7.4 ppbV,
472 respectively, and their ratios of RMSE and std on ~~the "Songshan" supercomputer~~[domestic cluster](#)
473 ~~A~~ are $5.8 \times 10^{-5}\%$, $4.8 \times 10^{-6}\%$, $5.7 \times 10^{-8}\%$, and $2.1 \times 10^{-4}\%$, which are smaller than two
474 NVIDIA clusters, especially much smaller than the NVIDIA V100 cluster. For example, the ratio
475 on the NVIDIA K40m cluster for four species are $1.2 \times 10^{-4}\%$, $6.6 \times 10^{-5}\%$, $7.0 \times 10^{-5}\%$, and
476 $4.1 \times 10^{-4}\%$, and ratio on the NVIDIA V100 cluster are $1.5 \times 10^{-2}\%$, $2.5 \times 10^{-3}\%$, $6.4 \times$
477 $10^{-3}\%$, and $1.3 \times 10^{-3}\%$, respectively.

478 ~~From AEs, REs, and ratio of RMSE and std between different CAMx versions, it can be~~
479 ~~identified that the HIP version of the GPU HADVPPM program runs on domestic cluster A with~~
480 ~~less difference, and the reason for this difference may be related to the fact that the NVIDIA GPU~~
481 ~~sacrifices part of the accuracy for improved computing performance. In other words, domestic~~
482 ~~cluster A are more accuracy for scientific computing in the field of the geoscience numerical~~
483 ~~models.~~

484 ~~[From AEs, REs, and ratio of RMSE and std between different CAMx versions, it is less](#)~~

485 difference that the GPU-HADVPPM4HIP program runs on the “Songshan” supercomputer.
 486 Because the simulation accuracy of geoscience numerical model is closely related to the model
 487 efficiency, and many model optimization works improve the computational performance by
 488 reducing the precision of the data, such as Vána et al. (2017) changed some variables precision in
 489 the atmospheric model from double precision to single precision, which increased the overall
 490 computational efficiency by 40%, and Wang et al. (2019) improved the computational efficiency
 491 of the gas-phase chemistry module in the air quality mode by 25%~28% by modifying the
 492 floating-point precision compile flag. Therefore, we speculate that this may be related to the
 493 manufacturing process of NVIDIA GPUs and domestic GPU-like accelerators, especially NIVIDA
 494 Tesla V100 series GPUs, which may use unknown optimizations to improve GPU performance
 495 efficiency by losing part of the accuracy. In this study, we mainly focus on numerical simulation.
 496 Of course, we also want to know the specific reasons for this, but we are not professional GPU
 497 research and development designers after all and do not know the underlying design logic of the
 498 hardware, so we can only present our experimental results in the air pollution model to you, and
 499 discuss with each other to jointly promote the application of GPU in the field of geoscience
 500 numerical models.

501 **Table 34.** The standard deviation (std) of O₃, PSO₄, CO and NO₂ on the Intel Xeon E5-2682 v4 CPU, root mean
 502 square error (RMSE) and its ratio on the NVIDIA V100 cluster, NVIDIA K40m cluster and “Songshan”
 503 supercomputer~~domestic cluster A~~

	std	NIVIDA V100 cluster		NIVIDA K40m cluster		<u>“Songshan”</u> <u>supercomputer</u> domestic <u>cluster A</u>	
		RMSE	RMSE/std	RMSE	RMSE/std	RMSE	RMSE/std
O₃ (ppbV)	9.6	1.5×10^{-3}	1.5×10^{-2}	1.1×10^{-5}	1.2×10^{-4}	7.4×10^{-6}	7.7×10^{-5}
PSO₄ ($\mu\text{g} \cdot \text{m}^{-3}$)	1.7	4.3×10^{-5}	2.5×10^{-3}	1.1×10^{-6}	6.6×10^{-5}	2.5×10^{-7}	1.5×10^{-5}
CO (ppbV)	141.9	9.0×10^{-3}	6.4×10^{-3}	1.0×10^{-4}	7.0×10^{-5}	4.4×10^{-7}	3.1×10^{-7}
NO₂ (ppbV)	7.4	9.3×10^{-5}	1.3×10^{-3}	3.0×10^{-5}	4.1×10^{-4}	2.0×10^{-5}	2.7×10^{-4}

504

505 4.3. Application performance

506 4.3.1. GPU-HADVPPM on a single GPU accelerator

507 ~~As described in Sect. 4.2, we validate the 48 hours simulation results outputted by the Fortran,~~
508 ~~CUDA, and HIP versions of CAMx. Next, computational performance was compared for the~~
509 ~~Fortran version of HADVPPM on the Intel Xeon E5-2682 v4 CPU and domestic CPU processor A,~~
510 ~~the CUDA version of GPU HADVPPM on the NVIDIA Tesla K40m and V100 GPU, and the HIP~~
511 ~~version of GPU HADVPPM on the domestic GPU-like accelerator A, under the BJ, HN and ZY~~
512 ~~case. The simulation time in this section is 1 hour unless otherwise specified. When evaluating the~~
513 ~~computational efficiency on different hardware platforms, the elapsed time of advection module~~
514 ~~launched two CPU processes on the domestic CPU processor A is taken as the benchmark, that is,~~
515 ~~the speedup is 1.0x. The runtime of the advection module on Intel CPU processor and different~~
516 ~~GPU accelerators is compared with the baseline to obtain the speedup. As described in Sect. 4.2,~~
517 ~~we validate the 48 hours simulation results outputted by the CAMx model which coupling the~~
518 ~~Fortran version HADVPPM, CUDA and HIP version of GPU HADVPPM. And then, the coupling~~
519 ~~computational performance of the Fortran version of HADVPPM on the Intel Xeon E5-2682 v4~~
520 ~~CPU and domestic CPU processor A, the CUDA version of GPU HADVPPM on the NVIDIA~~
521 ~~Tesla K40m and V100 GPU accelerators, and the HIP version of GPU HADVPPM on the~~
522 ~~domestic GPU-like accelerator A were compared under BJ, HN, and ZY case. The simulation time~~
523 ~~in this section is 1 hour unless otherwise specified.~~

524 ~~According to the results of Cao et al. (2023), the parallel design of the CAMx model adopts~~
525 ~~the primary/secondary mode, and Process0 (P0) is responsible for inputting and outputting the~~
526 ~~data and calling the MPI Barrier function to synchronize the process, and the other processes are~~
527 ~~responsible for simulation. When testing the computational performance of the advection module~~
528 ~~on the CPU, we only launch two CPU processes, namely P0 and Process1 (P1), where P0 is~~
529 ~~responsible for data input and output and synchronization process, and P1 is mainly responsible~~
530 ~~for simulation. In the P1 process, the system_clock functions in the Fortran language are used to~~
531 ~~test the elapsed time of the advection module on the CPU. Similarly, when testing the computation~~
532 ~~performance of the advection module on the GPU-like accelerator, we only launch 2 CPU~~

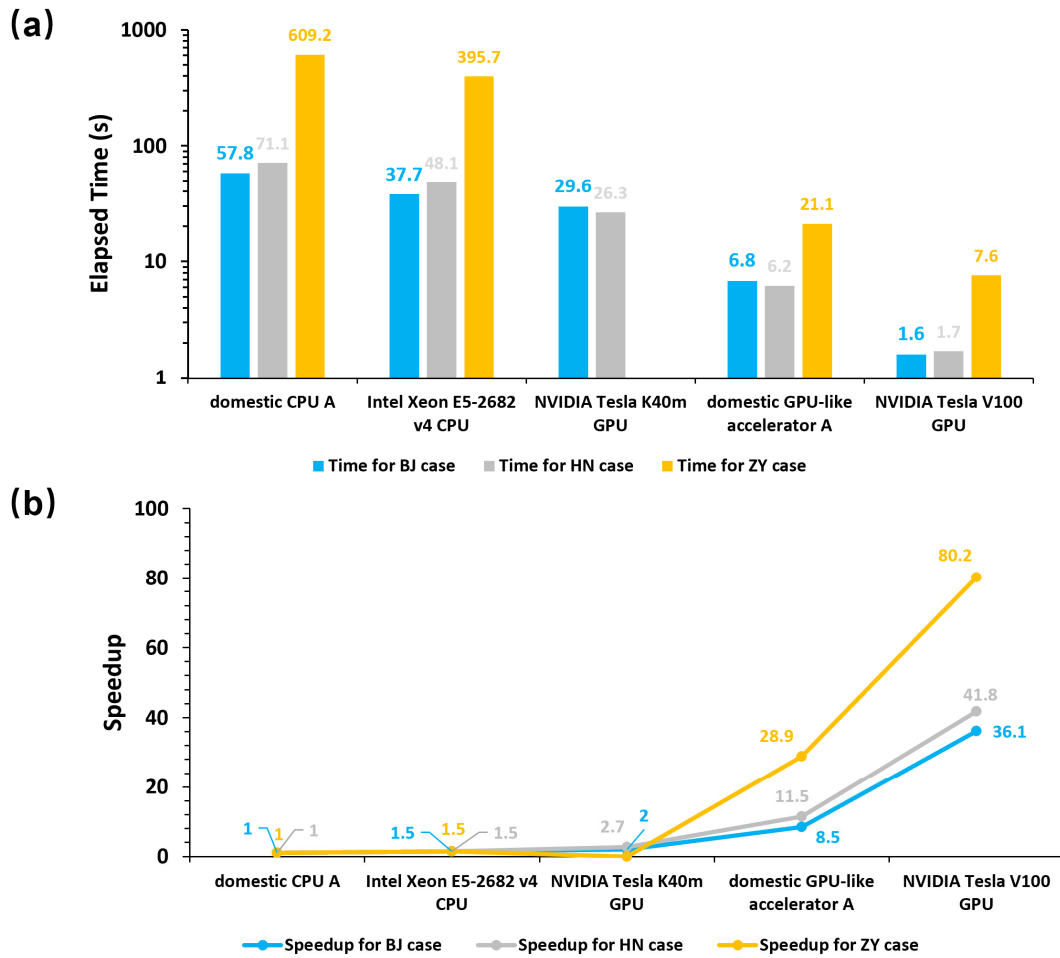
533 processes and 2 GPU-like accelerators. When a P1 process runs to the advection module, the
534 original computation process is migrated from the CPU to the GPU, and the hipEvent_t function
535 in HIP programming is used to test the running time of the advection module on the GPU-like
536 accelerator.

537 As described in Sect. 4.2, we validate the 48 hours simulation results outputted by the Fortran,
538 CUDA, and HIP versions of CAMx. Next, computational performance was compared for the
539 Fortran version of HADVPPM on the Intel Xeon E5-2682 v4 CPU and domestic CPU processor A,
540 the CUDA version of GPU-HADVPPM on the NVIDIA Tesla K40m and V100 GPU, and the HIP
541 version of GPU-HADVPPM on the domestic GPU-like accelerator A, under the BJ, HN and ZY
542 case. The simulation time in this section is 1 hour unless otherwise specified.

543 Similarity, since the CAMx model adopts the primary/secondary mode, two CPU processes
544 P0 and P1 are launched on the CPU, and the system clock functions in the Fortran language are
545 used to test the elapsed time of the advection module in P1 process. When testing the computation
546 performance of the advection module on the GPU-like accelerator, we also only launch 2 CPU
547 processes and 2 GPU-like accelerators. When a P1 process runs to the advection module, the
548 original computation process is migrated from the CPU to the GPU, and the hipEvent_t function
549 in HIP programming is used to test the running time of the advection module on the GPU-like
550 accelerator. When comparing the speedup on different GPU accelerators, the elapsed time of
551 advection module launched one CPU process (P1) on the domestic CPU processor A is taken as
552 the benchmark, that is, the speedup is 1.0x. The runtime of the advection module on Intel CPU
553 processor and different GPU accelerators is compared with the baseline to obtain the speedup.

554 Figure 65(a) and (b) shows the elapsed time and speedup of the different versions of
555 HADVPPM on the CPU processors and GPU accelerators for BJ, HN, and ZY cases, respectively.
556 The results show that using CUDA and HIP technology to port HADVPPM from CPU to GPU can
557 significantly improve its computational efficiency. For example, the elapsed time of the advection
558 module on the domestic processor A is 609.2 seconds under the ZY case. After it is ported to the
559 domestic GPU accelerator and NVIDIA V100 GPU, it only takes 21.1 seconds and 7.6 seconds to
560 complete the computing, and the speedups are 28.9x and 80.2x, respectively. The ZY case had the
561 largest number of grids in the three cases and exceeded the memory of a single NVIDIA Tesla

562 ~~K40m GPU accelerator, so it was not possible to test its elapsed time on it. Moreover, the~~
563 ~~optimization of thread and block co-indexing is used to simultaneously compute the grid point in~~
564 ~~the horizontal direction (Cao et al., 2023). Therefore, it can be seen from Fig. [ure 65](#)(b) that the~~
565 ~~larger the computing scale, the more obvious the acceleration, which indicates that GPU is more~~
566 ~~suitable for super-large scale parallel computing, and provides technical support for accurate and~~
567 ~~fast simulation of ultra-high-resolution air quality at the meter level in the future. Table 5 listed the~~
568 ~~elapsed time and speedup of the different versions of HADVPPM on the CPU processors and~~
569 ~~GPU accelerators for BJ, HN, and ZY cases. Using CUDA and HIP technology to port~~
570 ~~HADVPPM from CPU to GPU can significantly improve its computational efficiency. Moreover,~~
571 ~~the optimization of thread and block co-indexing is used to simultaneously compute the grid point~~
572 ~~in the horizontal direction (Cao et al., 2023), the larger the computing scale, the more obvious the~~
573 ~~acceleration. For example, for the BJ case, the elapsed time of HADVPPM on the domestic CPU~~
574 ~~processor A and Intel Xeon E5-2682 v4 CPU was 57.8 and 37.7 seconds, and it takes the only 29.6,~~
575 ~~6.8, and 1.6 seconds when porting to the NVIDIA Tesla K40m GPU, the domestic GPU-like~~
576 ~~accelerator A, and NVIDIA Tesla V100 GPU, with speedup of 2.0x, 8.5x, and 36.1x. The HN case~~
577 ~~has a slightly larger grid number, the acceleration of GPU HADVPPM on NVIDIA Tesla K40m~~
578 ~~GPU, the domestic GPU-like accelerator A, and NVIDIA Tesla V100 GPU is obvious which were~~
579 ~~2.7x, 11.5x, and 41.8x, respectively. The ZY case had the largest number of grids in the three cases~~
580 ~~and exceeded the memory of a single NVIDIA Tesla K40m GPU accelerator, so it was not~~
581 ~~possible to test its elapsed time on it. But as far as the domestic GPU-like accelerator A and~~
582 ~~NVIDIA Tesla V100 GPU are concerned, the ZY case gets 28.9x and 80.2x acceleration on it~~
583 ~~compared to the domestic CPU processor A.~~



584

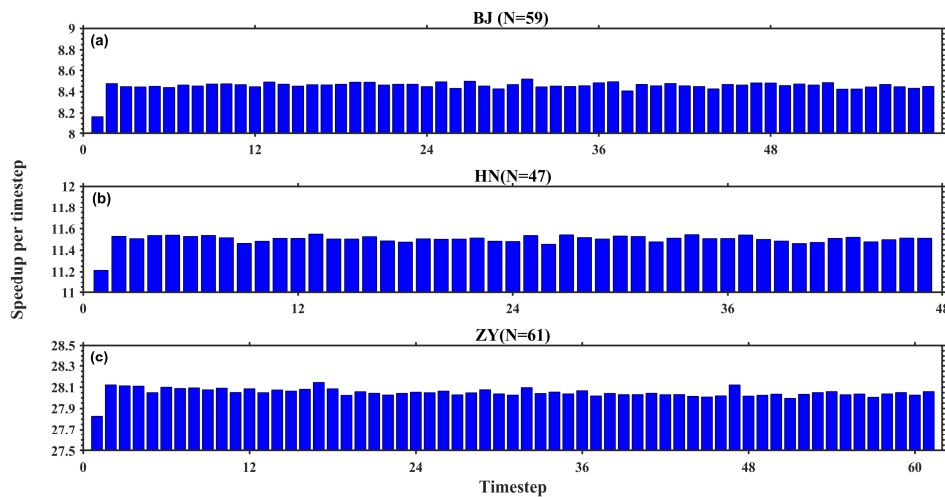
585 **Figure 65.** The elapsed time (a) and speedup (b) of the Fortran version of HADVPPM on the Intel Xeon E5-2682
 586 v4 CPU and the domestic CPU processor A, the CUDA version of GPU-HADVPPM on the NVIDIA Tesla K40m
 587 GPU, NVIDIA Tesla V100 GPU, and the HIP version of GPU-HADVPPM on the domestic GPU-like accelerator
 588 A for BJ, HN, and ZY case. The unit of elapsed time is in seconds (s).

589 **Table 5.** The elapsed time and speedup of the Fortran version of HADVPPM on the Intel Xeon E5-2682 v4 CPU
 590 and the domestic CPU processor A, the CUDA version of GPU-HADVPPM on the NVIDIA Tesla K40m GPU,
 591 NVIDIA Tesla V100 GPU, and the HIP version of GPU-HADVPPM on the domestic GPU-like accelerator A for
 592 BJ, HN, and ZY case. The unit of elapsed time is in seconds (s).

		BJ-case		HN-case		ZY-case	
		Elapsed time (s)	Speedup	Elapsed time (s)	Speedup	Elapsed time (s)	Speedup
CPU processor	domestic CPU processor A	57.8	1.0x	71.1	1.0x	609.2	1.0x
	Intel Xeon E5-2682 v4 CPU	37.7	1.5x	48.1	1.5x	395.7	1.5x
GPU accelerator	NVIDIA Tesla K40m	29.6	2.0x	26.3	2.7x	-	-

GPU						
domestic GPU-like accelerator A	6.8	8.5x	6.2	11.5x	21.1	28.9x
NVIDIA Tesla V100 GPU	1.6	36.1x	1.7	41.8x	7.6	80.2x

593 The timestep of BJ, HN and ZY case were 59, 47, and 61, respectively. Fig. 75 shows the
594 GPU-HADVPPM4HIP acceleration in each time step on a single domestic GPU-like accelerator A.
595 It can be seen from the figure that all three cases have the smallest speedup of 8.2x, 11.2x, and
596 27.8x at the first timestep, which is related to the time required for GPU-like accelerator startup.
597 When the GPU-like is started and operating normally, the speedup of the three cases tend to be
598 stable in the following time steps, and stabilize around 8.5x, 11.5x and 28.0x respectively.



599 Figure 75. The GPU-HADVPPM4HIP acceleration in each time step on a single GPU-like accelerator for BJ, HN,
600 and ZY case. The timestep of above three cases are 59, 47, and 61, respectively.

602 Table 46 further lists the total elapsed time of CAMx Fortran and HIP versions for BJ case
603 on the "Songshan" supercomputer and "Taiyuan" computing platform, and the computing time
604 of advection module with or without data transfer. By coupling the GPU-HADVPPM4HIP to
605 CAMx model and adopting a series of optimizations (Cao et al., 2023) such as communication
606 optimization, memory access optimization, and 2D thread optimization, the overall computation
607 time of CAMx-HIP model on a single domestic GPU-like accelerator is faster than that of the
608 original Fortran version on a single domestic CPU core. For example, on the "Songshan"
609 supercomputer, one hour of simulation in CAMx-HIP model takes 469 seconds, and the Fortran
610 version takes 481 seconds. On the "Taiyuan" computing platform, the acceleration effect is more

611 obvious due to the upgrade of hardware and network bandwidth, and the integration time of
612 CAMx-HIP model is 433 seconds when maintaining the same software environment, and the
613 integration time of the Fortran version is 453 seconds.

614 The elapsed time of GPU-HADVPPM given in Table 45 on NVIDIA GPU and domestic
615 GPU-like accelerator does not consider the data transfer time between CPU and GPU. However,
616 the communication bandwidth of data transfer between the CPU and GPU is one of the most
617 significant factors that restrict the performance of numerical model on the heterogeneous cluster
618 (Mielikainen et al., 2012; Mielikainen et al., 2013; Huang et al., 2013). To illustrate the significant
619 impact of CPU-GPU data transfer efficiency, the computational performance of GPU-HADVPPM
620 with and without data transfer time for the BJ case is tested on the “Songshan” supercomputer and
621 “Taiyuan” computing platform with the same DTK version 23.04 software environment and the
622 results are further presented in Table 6. For convenience of description, we refer to the execution
623 time of GPU-HADVPPM program on GPU kernel as kernel execution time, and the time of GPU-
624 HADVPPM running on GPU as total runtime, which contains two parts, namely, kernel execution
625 time and data transfer time between CPU and GPU.~~After testing, the kernel execution~~
626 ~~time and total running time of GPU-HADVPPM4HIP program on domestic GPU-like accelerator~~
627 ~~A are 6.8 seconds and 93.1 seconds, respectively, which means that only 7.3% of the time is spent~~
628 ~~on GPU computing, and the rest is spent on data transfer.~~ After testing, the kernel execution time
629 and total running time of GPU-HADVPPM4HIP program on domestic GPU-like accelerator A are
630 6.8 and 29.8 seconds, respectively. In other words, it only takes 6.8 seconds to complete the
631 computation on the domestic accelerator, but it takes 23.0 seconds to complete the data transfer
632 between the CPU and the domestic GPU-like accelerator, which is 3.4 times the computation time.
633 The same problem exists in the more advanced the “Taiyuan” computing platform, where the
634 GPU-HADVPPM4HIP takes only 5.7 seconds to complete the computation, while the data
635 transmission takes 18.2 seconds, which is 3.2 times the computation time.

636 By comparing the kernel execution time and total running time of GPU-HADVPPM4HIP on
637 the domestic accelerator, it can be seen that the data transfer efficiency between CPU and
638 GPU~~CPU-GPU~~ is really inefficient, which seriously restricts the computational performance of
639 numerical models in heterogeneous clusters. On the one hand, improving the data transfer

bandwidth between CPU and GPU. CPU-GPU can improve the computational efficiency of the model in heterogeneous clusters. On the other hand, the optimization measures can be implemented to improve the data transfer efficiency between CPU and GPU. For example, (1) Asynchronous data transfer is used to reduce the communication latency between CPU and GPU. Computation and data transfer are performed simultaneously to hide communication overhead; (2) Currently, some advanced GPU architectures support a unified memory architecture, so that the CPU and GPU can share the same memory space and avoid frequent data transfers. This reduces the overhead of data transfer and improves data transfer efficiency; (3) Cao et al. (2023) adopted communication optimization measures to reduce the communication frequency in one time integration step to one, but there is still the problem of high communication frequency in the whole simulation. In the future, we will consider porting other hotspots of CAMx model, or even the whole integral module except I/O, to GPU-like accelerators for increasing the proportion of code on the GPU and reduce the frequency of CPU-GPU communication.

Video memory and bandwidth are the two most significant factors affecting GPU performance, and high video memory and high bandwidth can better play the powerful computing performance of GPUs. Usually, the memory and bandwidth of the GPU are already given at the factory. In this case, the amount of data transferred to the GPU can be roughly estimated before the data is transferred to the GPU, and the amount of data transferred to the GPU can be adjusted according to the size of the GPU memory to ensure that the amount of data transferred to the GPU each time reaches the maximum GPU video memory, so as to give full play to the GPU performance more efficiently.

Table 46. The total elapsed time of CAMx Fortran and HIP versions for BJ case on the "Songshan" supercomputer and "Taiyuan" computing platform, and the computing time of advection module with or without data transfer. The unit of elapsed time is in seconds (s).

	"Songshan" supercomputer		"Taiyuan" computing platform	
	Fortran version	HIP version	Fortran version	HIP version
Total elapsed time	481.0	469.0	453.0	433.0
Computing time of advection module without data transfer	57.8	6.8	47.8	5.7
Computing time of advection module with data transfer	57.8	29.8	47.8	23.9

665 In the above experiments to test the coupling performance of GPU HADVPPM on NVIDIA
666 GPU and domestic GPU-like accelerator, the data transfer time between CPU and GPU was not
667 considered. However, the communication bandwidth of data transfer between the CPU and GPU is
668 one of the most significant factors that restrict the performance of numerical model on the
669 heterogeneous cluster (Mielikainen et al., 2012; Mielikainen et al., 2013; Huang et al., 2013). To
670 exhibit the significant impact of CPU-GPU data transfer efficiency, the coupled computing
671 performance of GPU HADVPPM with and without data transfer time for the BJ case is tested on
672 the domestic cluster A and B with the same DTK version 23.04 software environment. The
673 elapsed time of GPU HADVPPM on domestic GPU-like accelerator A with and without taking
674 into account the data transfer time between CPU and GPU are 6.8 and 93.1 seconds, respectively,
675 which means that only 7.3% of the time is spent on GPU computing, and the rest of the time is
676 spent on data transfer. Although, the domestic cluster B upgrade the hardware component and
677 network bandwidth, and the elapsed time of GPU HADVPPM on it with and without taking into
678 account the data transfer time are 5.7 and 23.9 seconds respectively, the GPU computing time is
679 still only 23.8%. Optimizing the data transfer efficiency between CPU and GPU is one of the most
680 important directions for the porting and adaptation of numerical models to heterogeneous clusters.

681 4.3.2. CAMx-HIP model on the heterogeneous cluster

682 Generally, the super large heterogeneous clusters have thousands of compute nodes which are
683 equipped with one or more GPUs on each node. To make full use of multiple GPUs, a parallel
684 architecture with an MPI and CUDA hybrid paradigm was implemented to improve the overall
685 computational performance of CAMx-CUDA model (Cao et al., 2023). In this studying, the hybrid
686 parallelism with an MPI and HIP paradigm was used to implement the HIP version of GPU-
687 HADVPPM run on multiple domestic GPU-like accelerators.

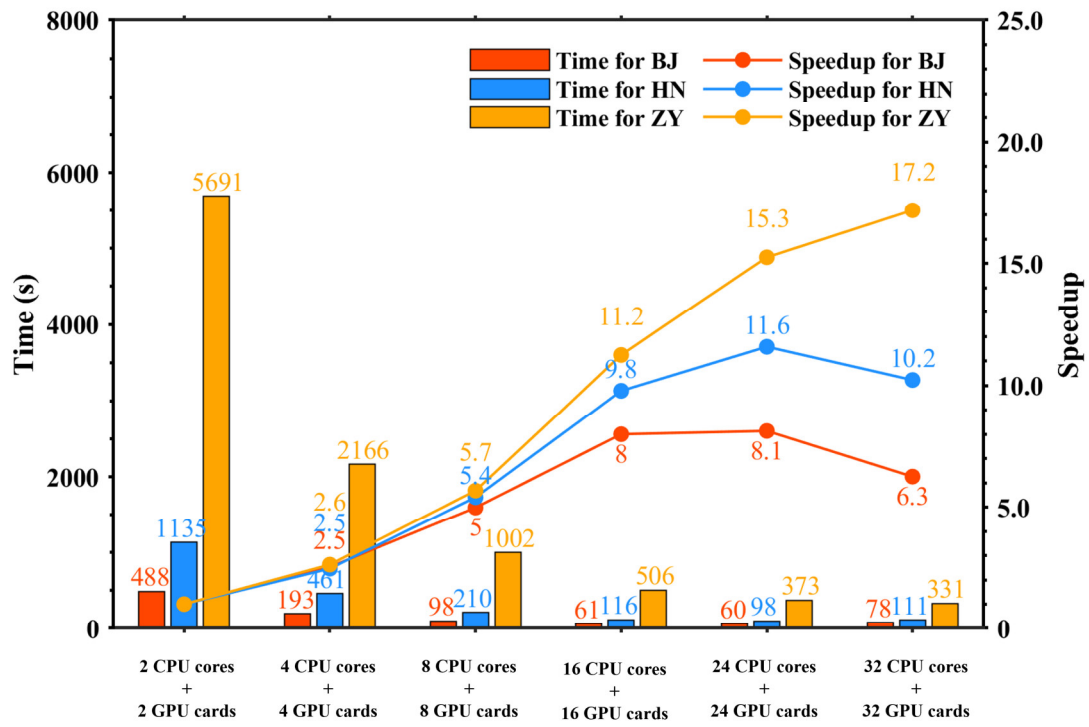
688 Fig.4 shows the total elapsed time and speedup of CAMx-HIP model which coupled with the
689 HIP version GPU HADVPPM on the domestic cluster A under the BJ, HN, and ZY cases. The
690 simulation of above three cases for one hour took 488 seconds, 1135 seconds and 5691 seconds
691 respectively when launching two domestic CPU processors and two GPU-like accelerators. When
692 the number of CPUs and GPUs reaches 24, the speedup of BJ and HN cases reaches the maximum,

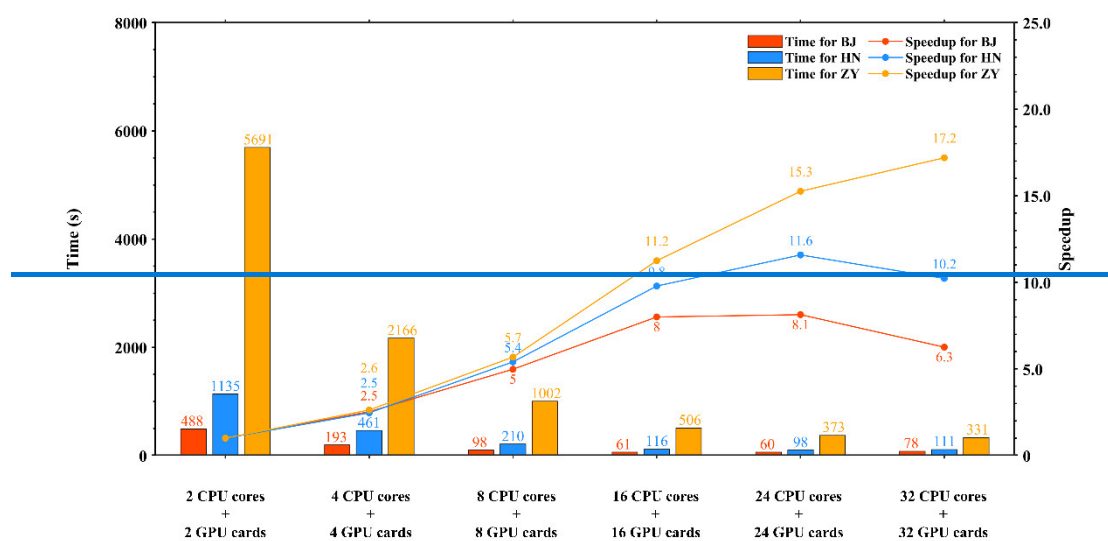
693 8.1x and 11.6x, respectively. In terms of the ZY case, it can achieve up to the 17.2 times speedup
694 when equipped with 32 domestic CPU processors and GPU-like accelerators.

695 Generally, the heterogeneous HPC systems have thousands of compute nodes which are
696 equipped with one or more GPUs on each compute node. To make full use of multiple GPUs, a
697 parallel architecture with an MPI and CUDA hybrid paradigm was implemented to improve the
698 overall computational performance of CAMx-CUDA model (Cao et al., 2023). In this studying,
699 the hybrid parallelism with an MPI and HIP paradigm was used to implement the HIP version of
700 GPU-HADVPPM run on multiple domestic GPU-like accelerators. Fig.86 shows the total elapsed
701 time and speedup of CAMx-HIP model which coupled with the HIP version GPU-HADVPPM on
702 the "Songshan" supercomputer under the BJ, HN, and ZY cases. The simulation of above three
703 cases for one hour took 488 seconds, 1135 seconds and 5691 seconds respectively when launching
704 two domestic CPU processors and two GPU-like accelerators. For the BJ and HN case, the
705 parallel scalability is highest when configured with 24 CPU cores and 24 GPU-like accelerators,
706 with speedup of 8.1x and 11.6x, respectively. In terms of the ZY case, due to its large number of
707 grids, the parallel scalability is the highest when 32 CPU cores and 24 GPU cards are configured,
708 and the acceleration ratio is 17.2x.

709 As mentioned above, data transfer between CPU and GPU takes several times more time
710 than computation. Regardless of the CPU-GPU data transfer consumption, GPU-HADVPPM4HIP
711 can achieve up to 28.9x speedup on a single domestic GPU-like accelerator. However, in terms of
712 the total time consumption, the CAMx-HIP model is only 10~20 seconds faster than the original
713 Fortran version when one GPU-like accelerator is configured. And as the number of CPU cores
714 and GPU-like accelerators increases, the overall computing performance of CAMx-HIP model is
715 lower than that of the original Fortran version. The main reason is related to the amount of data
716 transferred to GPU. As the number of MPI processes increases, the number of grids responsible
717 for each process decreases, and the amount of data transmitted by the advection module from CPU
718 to GPU decreases. However, GPUs are suitable for large-scale matrix computing. When the data
719 scale is small, the performance of GPU is low, and the communication efficiency between CPU
720 and GPU is the biggest bottleneck (Cao et al., 2023). Therefore, the computational
721 performance of CAMx-HIP model is not as good as the original Fortran version when MPI

722 processes increase. According to the characteristics of GPUs suitable for large-scale matrix
 723 computing, the model domain can be expanded and the model resolution can be increased in the
 724 future to ensure that the amount of data transferred to each GPU reaches the maximum video
 725 memory occupation, so as to make efficient use of GPU. In addition, the advection module only
 726 accounts for about 10% of the total time consumption in CAMx model (Cao et al., 2023), and in
 727 the future, it is considered to port the entire integration module except I/O to the GPU to minimize
 728 the communication frequency.



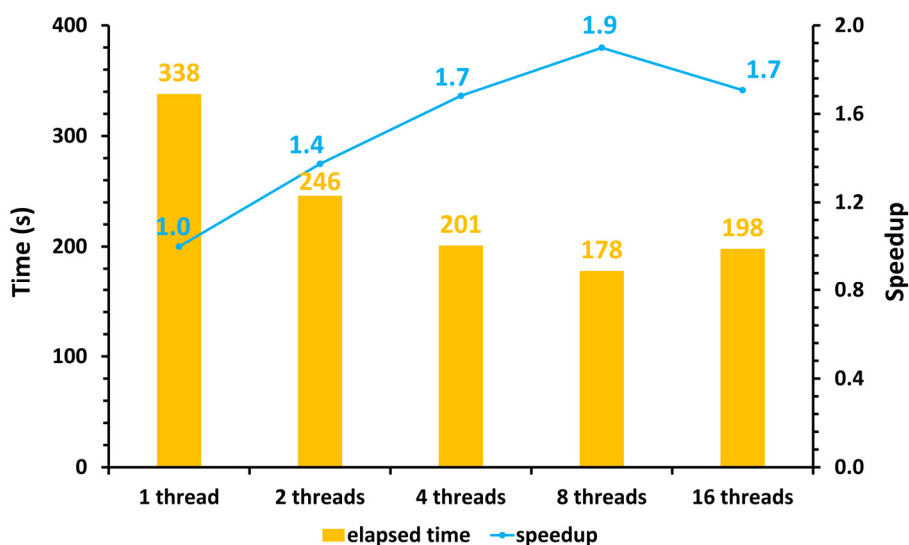


731
732 **Figure 864.** The total elapsed time and speedup of CAMx-HIP model on the "Songsshan" supercomputer
733 domestic cluster A under the BJ, HN, and ZY cases. The unit is in seconds (s).

734 The number of GPU accelerators in a single compute node is usually much smaller than the
735 number of CPU cores in the heterogeneous HPC systemssuper-large heterogeneous cluster. Using
736 the hybrid parallel paradigm with MPI and HIP to configure one GPU accelerator for each CPU
737 process results in idle computing resources for the remaining CPU cores. Therefore, the multi-
738 level hybrid parallelism scheme was introduced to further improve the total computational
739 performance of the CAMx-HIP model. As described in the Sect. 3.2, the horizontal advection
740 module is accelerated by MPI and HIP technology, and the other modules, such as photolysis
741 module, deposition module, chemical module, etc., which runs on the CPU are accelerated by MPI
742 and OMP under the framework of the multi-level hybrid parallelism.~~Using the hybrid parallel~~
743 ~~paradigm with MPI and HIP to configure one GPU accelerator for each CPU process results in~~
744 ~~idle computing resources for the remaining CPU cores. Therefore, the multi-level hybrid~~
745 ~~parallelism scheme was introduced to further improve the total computational performance of the~~
746 ~~CAMx-HIP model. As described in the Sect. 3.2, the horizontal advection module is accelerated~~
747 ~~by MPI and HIP technology and the other modules which runs on the CPU are accelerated by MPI~~
748 ~~and OMP under the framework of the multi-level hybrid parallelism.~~

749 The ZY case achieved the maximum speed-up when launching the 32 domestic CPU
750 processors and GPU-like accelerators. In the same configuration, Fig. 975 shows the total elapsed

751 time and speedup of CAMx-HIP model when further implementing the multi-level hybrid
 752 parallelism on the "Songshan" supercomputer ~~the domestic cluster A~~. The AEs of the simulation
 753 results between the CAMx-HIP model and CAMx-HIP model with the OMP technology is within
 754 ± 0.04 ppbV, and the specified results are shown in Figure S1. As the number of threads increases,
 755 the elapsed time of CAMx-HIP model is further reduced. When a CPU core launching 8 threads,
 756 the one-hour integration time in CAMx-HIP model has been reduced from 338 seconds to 178
 757 seconds, with a maximum acceleration of 1.9x.



758
 759 **Figure 975.** The total elapsed time and speedup of CAMx-HIP model when implementing the multi-level hybrid
 760 parallelism in the ZY case. The unit is in seconds (s).

761 5. Conclusions and discussion

762 GPUs have become an essential part of providing processing power for high performance
 763 computing applications, especially in the field of geoscience numerical models, implementing
 764 super-large scale parallel computing of numerical models on GPUs has become one of the
 765 significant directions of its future development. ~~GPUs have become an essential part of providing~~
 766 ~~processing power for high performance computing application, especially in the field of~~
 767 ~~geoscience numerical models, implementing super-large scale parallel computing of numerical~~
 768 ~~models on GPUs has become one of the significant directions of its future development.~~ In this

769 study, the ROCm HIP technology was implemented to port the GPU-HADVPPM from the
770 NVIDIA GPUs to China's domestically GPU-like accelerators, and further introduced the multi-
771 level hybrid parallelism scheme to improve the total computational performance of the CAMx-
772 HIP model on the China's domestically heterogeneous cluster.~~In this studying, the ROCm HIP~~
773 ~~technology was implemented to port the GPU-HADVPPM from the NVIDIA GPUs to China's~~
774 ~~domestically GPU-like accelerators, and further introduced the multi-level hybrid parallelism~~
775 ~~scheme to improve the total computational performance of the CAMx-HIP model on the China's~~
776 ~~domestically heterogeneous cluster.~~

777 The consistency of model simulation results is a significant prerequisite for heterogeneous
778 porting, although the experimental results show that the deviation between the CUDA version and
779 the Fortran version of CAMx model, and the deviation between the HIP version and the Fortran
780 version of CAMx model, are within the acceptable rang, the simulation difference between the
781 HIP version of CAMx model and Fortran version of CAMx model is smaller.~~The consistency of~~
782 ~~model simulation results is a significant prerequisite for heterogeneous porting, although the~~
783 ~~experimental results show that the simulation difference of CAMx-CUDA and CAMx-HIP models~~
784 ~~are within an acceptable range, the simulation difference of CAMx-HIP model is smaller, which~~
785 ~~indicates that the domestic GPU-like accelerator is more accuracy for scientific computing in the~~
786 ~~field of geoseience numerical models. Moreover, the BJ, HN, and ZY test cases can achieve 8.5x,~~
787 ~~11.5x, and 28.9x speedup, respectively, when the HADVPPM program is ported from the~~
788 ~~domestic CPU processor A to the domestic GPU-like accelerator A.~~~~Moreover, the BJ, HN, and ZY~~
789 ~~test cases can achieve 8.5x, 11.5x, and 28.9x speedup, respectively, when the GPU-HADVPPM~~
790 ~~program is ported to the domestic GPU-like accelerator A. The experimental results of different~~
791 ~~cases show that the larger the computing scale, the more obvious the acceleration effect of the~~
792 ~~GPU-HADVPPM program, indicating that GPU is more suitable for super-large scale parallel~~
793 ~~computing, and provides technical support for accurate and fast simulation of ultra-high-resolution~~
794 ~~air quality at the meter level in the future.~~~~And the larger the computing scale, the more obvious the~~
795 ~~acceleration effect of the GPU-HADVPPM program, which means that the GPU is more suitable~~
796 ~~for super-large scale parallel computing. The data transfer bandwidth between CPU and GPU is~~
797 ~~one of the most important factors affecting the computational efficiency of numerical model in~~

798 heterogeneous clusters, as shown by the fact that the elapsed time of GPU-HADVPPM program
799 on GPU only accounts for 7.3% and 23.8% when considering the data transfer time between CPU
800 and GPU on the the “Songshan” supercomputer and “Taiyuan” computing platform. Therefore,
801 optimizing the data transfer efficiency between CPU and GPU is one of the important directions
802 for the porting and adaptation of geoscience numerical models on heterogeneous clusters in the
803 future. The data transfer bandwidth between CPU and GPU is one of the most important factors
804 affecting the computational efficiency of numerical model in heterogeneous clusters, the elapsed
805 time of GPU HADVPPM program on GPU only accounts for 7.3% and 23.8% when considering
806 the data transfer time between CPU and GPU on the domestic cluster A and B. Therefore,
807 optimizing the data transfer efficiency between CPU and GPU is one of the important directions
808 for the porting and adaptation of geoscience numerical models on heterogeneous clusters in the
809 future.

810 There is still potential to further improve the computational efficiency of the CAMx-HIP
811 model in the further. First, improve the data transfer efficiency of GPU-HADVPPM between the
812 CPU and the GPU and reduce the data transfer time. Secondly, increase the proportion of HIP C
813 code in CAMx-HIP model on the domestic GPU-like accelerator, and port other modules of
814 CAMx-HIP model to the domestic GPU-like accelerator for computing. Finally, the data type of
815 some variables could be changed from double precision to single precision, and the mixing-
816 precision method is used to further improve the CAMx-HIP computing performance.~~Finally, the~~
817 ~~data type of some variables can be changed from double precision to single precision, and the~~
818 ~~mixing precision method is used to further improve the CAMx-HIP computing performance.~~

819
820
821 *Code and data availability.* The source codes of CAMx version 6.10 are available at [https://camx-](https://camx-wp.azurewebsites.net/download/source/)
822 [wp.azurewebsites.net/download/source/](https://camx-wp.azurewebsites.net/download/source/) (ENVIRON, 2023). The datasets related to this paper and
823 the CAMx-HIP codes are available online via ZENODO
824 (<https://doi.org/10.5281/zenodo.10158214>), and the CAMx-CUDA code is available online via
825 ZENODO (<https://doi.org/10.5281/zenodo.7765218>, Cao et al., 2023).

826

827 *Author contributions.* KC and QW conducted the simulation and prepared the materials. QW, LiW
828 and LaW planned and organized the project. KC, QW, HG, HW, XT and LL refactored and
829 optimized the codes. LiW, NW, HC, [DXL](#) and [DQL](#) collected and prepared the data for the
830 simulation. KC, HW, QW, and HG validated and discussed the model results. KC, QW, LiW, NW,
831 XT, HG, and LaW took part in the discussion.

832

833 *Competing interests.* The authors declare that they have no conflict of interest.

834

835 *Acknowledgements.* The National Key R&D Program of China (grant no. 2020YFA0607804), the
836 National Supercomputing Center in Zhengzhou Innovation Ecosystem Construction Technology
837 Special Program (grant no. 201400210700), GHfund A (grant no. 202302017828), and the Beijing
838 Advanced Innovation Program for Land Surface funded this work. The authors would like to
839 thank the High Performance Scientific Computing Center (HSCC) of Beijing Normal University
840 for providing some high-performance computing environment and technical support.

841

842 **Reference**

843 Alvanos, M. and Christoudias, T.: GPU-accelerated atmospheric chemical kinetics in the
844 ECHAM/MESSy (EMAC) Earth system model (version 2.52), Geoscientific Model
845 Development, 10, 3679-3693, 10.5194/gmd-10-3679-2017, 2017.

846 AMD: ROCm Documentation Release 5.7.1,
847 https://rocm.docs.amd.com/_downloads/en/latest/pdf/ (last access: 20 October 2023), 2023.

848 Bott, A.: A Positive Definite Advection Scheme Obtained by Nonlinear Renormalization of the
849 Advective Fluxes, Monthly Weather Review - MON WEATHER REV, 117, 10.1175/1520-
850 0493(1989)117<1006:APDASO>2.0.CO;2, 1989.

851 [CAMx, A multi-scale photochemical modeling system for gas and particulate air pollution,](#)
852 [available at: https://www.camx.com/](https://www.camx.com/) (last access: 20 October 2023), 2023.

853 Cao, K., Wu, Q., Wang, L., Wang, N., Cheng, H., Tang, X., Li, D., and Wang, L.: GPU-
854 HADVPPM V1.0: a high-efficiency parallel GPU design of the piecewise parabolic method

855 (PPM) for horizontal advection in an air quality model (CAMx V6.10), *Geosci. Model Dev.*,
856 16, 4367-4383, 10.5194/gmd-16-4367-2023, 2023.

857 Cao, K., Wu, Q., Wang, L., Wang, N., Cheng, H., Tang, X., Li, D., and Wang, L.: The dataset of the
858 manuscript “GPUHADVPPM V1.0: high-efficient parallel GPU design of the Piecewise
859 Parabolic Method (PPM) for horizontal advection in air quality model (CAMx V6.10)”,
860 Zenodo [data set], <https://doi.org/10.5281/zenodo.7765218>, 2023.

861 Colella, P. and Woodward, P. R.: The Piecewise Parabolic Method (PPM) for gas-dynamical
862 simulations, *Journal of Computational Physics*, 54, 174-201, [https://doi.org/10.1016/0021-](https://doi.org/10.1016/0021-9991(84)90143-8)
863 9991(84)90143-8, 1984.

864 ENVIRON: User Guide for Comprehensive Air Quality Model with Extensions Version 6.1,
865 https://camx-wp.azurewebsites.net/Files/CAMxUsersGuide_v6.10.pdf (last access: 20
866 October 2023), 2014.

867 ENVIRON: CAMx version 6.1, ENVIRON [code], available at: [https://camx-](https://camx-wp.azurewebsites.net/download/source/)
868 [wp.azurewebsites.net/download/source/](https://camx-wp.azurewebsites.net/download/source/), last access: 20 October 2023.

869 Huang, M., Huang, B., Mielikainen, J., Huang, H. L. A., Goldberg, M. D., and Mehta, A.: Further
870 Improvement on GPU Based Parallel Implementation of WRF 5-Layer Thermal Diffusion
871 Scheme, in: 2013 International Conference on Parallel and Distributed Systems, Seoul, South
872 Korea, 15–18 December 2013, <https://doi.org/10.1109/icpads.2013.126>, 2013.

873 Linford, J. C., Michalakes, J., Vachharajani, M., and Sandu, A.: Automatic Generation of
874 Multicore Chemical Kernels, *IEEE Transactions on Parallel and Distributed Systems*, 22,
875 119-131, 10.1109/tpds.2010.106, 2011.

876 Mielikainen, J., Huang, B., Huang, H.-L. A., and Goldberg, M. D.: GPU Implementation of Stony
877 Brook University 5-Class Cloud Microphysics Scheme in the WRF, *IEEE Journal of Selected*
878 *Topics in Applied Earth Observations and Remote Sensing*, 5, 625-633,
879 10.1109/jstars.2011.2175707, 2012.

880 Mielikainen, J., Huang, B., Wang, J., Allen Huang, H. L., and Goldberg, M. D.: Compute unified
881 device architecture (CUDA)-based parallelization of WRF Kessler cloud microphysics
882 scheme, *Computers & Geosciences*, 52, 292-299, 10.1016/j.cageo.2012.10.006, 2013.

883 [News, Frontier Remains as Sole Exaflop Machine and Retains Top Spot, Improving Upon Its](#)

884 [Previous HPL Score, available at: https://www.top500.org/news/frontier-remains-sole-](https://www.top500.org/news/frontier-remains-sole-)
885 [exaflop-machine-and-retains-top-spot-improving-upon-its-previous-hpl-score/](https://www.top500.org/news/frontier-remains-sole-exaflop-machine-and-retains-top-spot-improving-upon-its-previous-hpl-score/) (last access:
886 [20 October 2023](https://www.top500.org/news/frontier-remains-sole-exaflop-machine-and-retains-top-spot-improving-upon-its-previous-hpl-score/)), 2023.

887 NVIDIA: CUDA C++ Programming Guide Version 10.2,
888 https://docs.nvidia.com/cuda/archive/10.2/pdf/CUDA_C_Programming_Guide.pdf (last
889 access: 20 October 2023), 2020.

890 Odman, M. and Ingram, C.: Multiscale Air Quality Simulation Platform (MAQSIP): Source Code
891 Documentation and Validation, 1996.

892 [ROCm, AMD ROCm-HIP documentation, available at: https://rocm.docs.amd.com/en/docs-5.0.0](https://rocm.docs.amd.com/en/docs-5.0.0)
893 [\(last access: 20 October 2023\)](https://rocm.docs.amd.com/en/docs-5.0.0), 2023.

894 Sun, J., Fu, J. S., Drake, J. B., Zhu, Q., Haidar, A., Gates, M., Tomov, S., and Dongarra, J.:
895 Computational Benefit of GPU Optimization for the Atmospheric Chemistry Modeling,
896 Journal of Advances in Modeling Earth Systems, 10, 1952-1969,
897 <https://doi.org/10.1029/2018MS001276>, 2018.

898 [Top500, Supercomputing Top500 list, available at: https://www.top500.org/lists/top500/2023/06/](https://www.top500.org/lists/top500/2023/06/)
899 [\(last access: 20 October 2023\)](https://www.top500.org/lists/top500/2023/06/), 2023.

900 [Váňa, F., Düben, P., Lang, S., Palmer, T., Leutbecher, M., Salmond, D., and Carver, G.: Single](https://doi.org/10.1175/mwr-d-16-0228.1)
901 [Precision in Weather Forecasting Models: An Evaluation with the IFS, Mon. Weather](https://doi.org/10.1175/mwr-d-16-0228.1)
902 [Rev.,145, 495–502, https://doi.org/10.1175/mwr-d-16-0228.1, 2017.](https://doi.org/10.1175/mwr-d-16-0228.1)

903 [Wang, H., Lin, J., Wu, Q., Chen, H., Tang, X., Wang, Z., Chen, X., Cheng, H., and Wang, L.: MP](https://doi.org/10.5194/gmd-12-749-2019)
904 [CBM-Z V1.0: design for a new Carbon Bond Mechanism Z \(CBM-Z\) gas-phase chemical](https://doi.org/10.5194/gmd-12-749-2019)
905 [mechanism architecture for next-generation processors, Geosci. Model Dev., 12, 749–764,](https://doi.org/10.5194/gmd-12-749-2019)
906 [https://doi.org/10.5194/gmd-12-749-2019, 2019.](https://doi.org/10.5194/gmd-12-749-2019)

907 Wang, P., Jiang, J., Lin, P., Ding, M., Wei, J., Zhang, F., Zhao, L., Li, Y., Yu, Z., Zheng, W., Yu, Y.,
908 Chi, X., and Liu, H.: The GPU version of LASG/IAP Climate System Ocean Model version 3
909 (LICOM3) under the heterogeneous-compute interface for portability (HIP) framework and
910 its large-scale application, [Geosci. Model Dev., GEOSCIENTIFIC—MODEL](https://doi.org/10.5194/gmd-14-2781-2021)
911 [DEVELOPMENT](https://doi.org/10.5194/gmd-14-2781-2021), 14, 2781-2799, 10.5194/gmd-14-2781-2021, 2021.